Technical Report

TR-10-66

Corrosion calculations report for the safety assessment SR-Site

Svensk Kärnbränslehantering AB

December 2010

Svensk Kärnbränslehantering AB
Swedish Nuclear Fuel
and Waste Management Co

Box 250, SE-101 24 Stockholm
Phone +46 8 459 84 00

ISSN 1404-0344
SKB TR-10-66

Corrosion calculations report for the safety assessment SR-Site

Svensk Kärnbränslehantering AB

December 2010

Keywords: SKBdoc 1271919, Canister, Copper, Corrosion, Erosion, Mass balance, Mass transport.

Preface

This document describes calculations of copper corrosion phenomena relevant for a KBS-3 repository. The calculations were made as part of the safety assessment SR-Site that supports SKB's license application for a final repository for spent nuclear fuel at Forsmark, Sweden.

The corrosion calculations are a further development of the corresponding calculations in the SR-Can safety assessment (SKB TR-06-09). The calculations for SR-Site are presented in the SR-Site main report (SKB TR-11-01) and in the Fuel and canister process report (SKB TR-10-46). This report is a compilation giving further details of the calculations and was made by Christina Lilja, SKB.

The report has been reviewed by Jordi Bruno, Amphos, Spain and Ivars Neretnieks, Royal Institute of Technology, Sweden.

Stockholm, December 2010

Allan Hedin
Project leader SR-Site

Summary

This report is a compilation of the quantitative assessments of corrosion of the copper canisters in a KBS-3 repository. The calculations are part of the safety assessment SR-Site that is the long-term safety assessment to support the license application for building a final repository for spent nuclear fuel at Forsmark, Sweden.

The safety assessment methodology gives the frame for the structured and documented approach to assess all conceivable corrosion processes. The quantitative assessments are done in different ways depending on the nature of the process and on the implications for the long-term safety.

The starting point for the handling of the corrosion processes is the description of all known corrosion processes for copper with the current knowledge base and applied to the specific system and geology. Already at this stage some processes are excluded for further analysis, for example if the repository environment is not a sufficient prerequisite for the process to occur. The next step is to identify processes where the extent of corrosion could be bounded, e.g. by a mass balance approach. For processes where a mass balance is not limiting, the mass transport of corrodants (or corrosion products) is taken into account. A simple approach would be just to calculate the diffusive transport of corrodants through the bentonite, but generally the transport resistance for the interface between groundwater in a rock fracture intersecting the deposition hole and the bentonite buffer is more important. In SR-Site, the concept of equivalent flowrate, Q_{eq}, is used. This assessment is done integrated with the evaluation of the geochemical and hydrogeological evolution of the repository.

For most of the corrosion processes analysed, the corrosion depth is much smaller than the copper shell thickness, even for the assessment time of 10^6 years. Several processes give corrosion depths less than 100 μm, but no process give corrosion depths larger than a few millimetres. The corrosion depths from the different processes could not simply be summed up as their combination requires a far more detailed chemical analysis (as well as statistical analysis regarding the flow and sulphide distributions), but, even if they are cautiously added, the sum is still less than 5 mm.

For the case of a partially eroded buffer, the probabilistic calculations show that corrosion could lead to penetration of the copper shell for on average less than one canister. Such corrosion extent only comes about for canisters experiencing the most unfavourable combinations of sulphide concentration and flow rates. The calculations give a span of number of failed canisters from zero to less than two penetrated canisters which covers uncertainties regarding the buffer erosion process, the variability in the hydrogeological DFN models and uncertainties in the assumed sulphide concentration distribution, as well as uncertainties in the conceptual model of corrosion geometry (the part of the copper surface that is corroded by the sulphide transported to the canister).

Sammanfattning

Den här rapporten är en sammanställning av kvantitativa bedömningar av korrosion på kopparkapslar i ett KBS-3-förvar. Beräkningarna är en del av säkerhetsanalysen SR-Site som är den analys för långsiktig säkerhet som är ett underlag till ansökan om tillstånd för att bygga ett slutförvar för använt bränsle i Forsmark.

Metodiken för säkerhetsanalysen ger ramarna för den strukturerade och dokumenterade ansatsen som används för att utvärdera alla tänkbara korrosionsprocesser. Den kvantitativa bedömningen görs på olika sätt beroende på typen av process och på implikationerna för långsiktig säkerhet.

Utgångspunkten för hanteringen av korrosionsprocesserna är beskrivningen av alla kända korrosionsprocesser för koppar byggt på den befintliga kunskapsbasen och för det specifika systemet och geologin. Redan på detta stadium kan en del processer uteslutas från den fortsatta analysen, till exempel om förvarsmiljön inte innebär en tillräcklig förutsättning för att processen ska uppträda. Nästa steg är att identifiera processer där omfattningen av korrosionen kan anges som begränsad, till exempel genom en massbalansberäkning. För processer där en massbalans inte är begränsande, används en ansats med begränsning genom masstransport av korrodanter (eller korrosionsprodukter). I ett enkelt fall beräknas enbart den diffusiva transporten genom bentoniten, men vanligtvis är transportmotståndet i överföringen mellan grundvattnet i en spricka i berget (som korsar deponeringshålet) och bentonitbufferten viktigare. För det fallet används i SR-Site konceptet med ekvivalent flöde, Q_{eq}. Analysen görs integrerat med utvärderingen av den geokemiska och hydrogeologiska utvecklingen hos förvaret.

För de flesta av de analyserade processerna är korrosionsdjupet mycket mindre än koppartjockleken, även för analystiden 10^6 år. Flera processer ger korrosionsdjup som är mindre än 100 µm, men ingen process ger korrosionsdjup större än några få millimeter. Korrosionsdjupet från de olika processerna kan inte enkelt summeras, eftersom det krävs en avsevärt mer detaljerad kemisk analys för att kombinera dem (liksom en statistisk analys för flödes- och sulfidfördelningar), men, även om de försiktigtvis summeras, är summan fortfarande mindre än 5 mm.

I fallet med en delvis eroderad buffert, visar de probabilistiska beräkningarna att korrosionen leder till genombrott i kopparhöljet för i medeltal mindre än en kapsel. Korrosion i den omfattningen kan bara inträffa för kapslar som utsätts för de mest ogynnsamma kombinationerna av sulfidkoncentration och flödeshastighet. Beräkningarna ger ett spann för antalet genomkorroderade kapslar som sträcker sig från noll till mindre än två genomkorroderade kapslar. Detta täcker osäkerheter i bufferterosionsprocessen, variabiliteten in den hydrogeologiska DFN-modellen och osäkerheter i den använda sulfidkoncentrationsfördelningen, liksom osäkerheter i den konceptuella modellen för korrosionsgeometrin (den del av kopparytan som korroderas av sulfiden som transporteras till kapseln).

Contents

1 Introduction

1.1 Aims and scope

This report is a compilation of the quantitative assessments related to potential corrosion of the copper canisters in a KBS-3 repository. The calculations are part of the safety assessment SR-Site, the long-term safety assessment to support the license application for building a final repository for spent nuclear fuel at Forsmark, Sweden.

The quantitative assessments are done in different ways depending on the nature of the process and on the implications for the long-term safety. This means that the calculations are at a different level of detail, which is a result of the strategy for an efficient assessment of the various corrosion mechanisms.

1.2 Assessment methodology

The safety assessment methodology gives the framework for the structured and documented approach to assess all conceivable corrosion processes. The central report to describe the corrosion processes is the Fuel and canister process report /SKB 2010a/, where the general knowledge base of corrosion mechanisms is described and then applied to the KBS-3 system. The further handling of the processes in the safety assessment is given in that report as well. All the processes are treated qualitatively and some also quantitatively in the process report.

As the treatment of the processes varies, the different parts of this report have different roles:

- For the processes that are quantitatively treated in the process report the calculations are repeated here, with emphasis on equations and parameter values used.
- For especially the corrosion by sulphide the assessment must be done integrated with the evaluation of the geochemical and hydrogeological evolution of the repository. This evaluation is done in the main report for SR-Site /SKB 2011/. For the evaluations performed with mass balances and simple 1-dimensional diffusion calculations the quantitative assessment is repeated here, with some more details.
- For the evaluation of sulphide in the groundwater (and the possibly intruding oxygen rich glacial melt water) the assessment is done with mass transport models using flow distributions from the hydrogeological modelling within SR-Site. For these models the current report documents the used equations and the implementation in the calculational code (in Excel) as well as gives the results, most of which are used in the main report for SR-Site and the radionuclide transport report /SKB 2010b/.

The qualification of data to SR-Site is generally done in the Data report /SKB 2010c/. The corrosion parameter with a thorough treatment in that report is the derivation of the minimum copper thickness at emplacement.

1.3 Structure of the report

The structure of the report is as follows. Chapter 2 describes the KBS-3 canister design, while Chapter 3 elaborates on the strategy for the corrosion assessment. In Chapter 4 the mass transport models are derived, starting with simple 1D diffusion and then going into diffusive and advective transport in fractured rock, for an intact buffer and for a partially eroded buffer. Chapter 5 gives the qualitative assessment for the different corrosion processes driven by gamma radiation, oxygen and sulphide. Also included is a what-if calculation on corrosion by water in anoxic water. In Chapter 6 the conclusions for the assessment of corrosion in SR-Site are summarised. Appendices give the notation and data used, and the documentation of input and resulting output files used in the SR-Site corrosion calculations.

2 Copper canister design

A repository for spent nuclear fuel is planned to be located at 470 m depth in Forsmark /SKB 2011/. The fuel is to be enclosed in canisters consisting of a load-bearing cast iron insert and a copper shell as corrosion barrier. The canister will be surrounded by a bentonite clay barrier and placed in individual deposition holes drilled from the floor of a tunnel system in the granitic bedrock. The canister, the bentonite buffer and the rock are the main constituents of the KBS-3 concept for deposition of nuclear waste.

The canister is designed to withstand the mechanical loads in the repository, comprising isostatic loads, the load from shear movements and asymmetric loads. The canister should further resist corrosion so that the number of failed canisters due to corrosion does not exceed what is acceptable with respect to the risk criterion for 100,000 years /SKB 2009/.

The canister reference design has an insert to withstand the mechanical loads and a copper shell to provide corrosion resistance, with the components as shown in Figure 2-1. The insert is manufactured of nodular cast iron with steel channel tubes in which the fuel assemblies are to be positioned. The channel tubes are made from square profiled steel tubes welded together to form a steel tube cassette which is placed in the casting mould. The insert is closed by a steel lid tightened with a central screw.

In order to conform to the design premises regarding the corrosion loads, the copper shell, i.e. tube, lid and base, are made of oxygen-free copper doped with 30–100 ppm phosphorus (Cu-OFP) /SKB 2010d/. The copper base and lid are welded to the copper tube by friction stir welding (FSW).
To facilitate handling of the canister, the copper lid is provided with a flange to allow handling equipment to grip the canister. The main design feature to be analysed in this report is the copper shell thickness, for which the design premise is expressed as “a nominal copper thickness of 5 cm, also considering the welds” /SKB 2009/. The copper thickness used in the corrosion calculations is further discussed in Section 4.3.4.

The outer dimensions of the copper shell are the height (including the lifting flange) and the radius /SKB 2010d/:

$h_{Cu} = 4.835\ m$

$r_{Cu} = 0.525\ m$

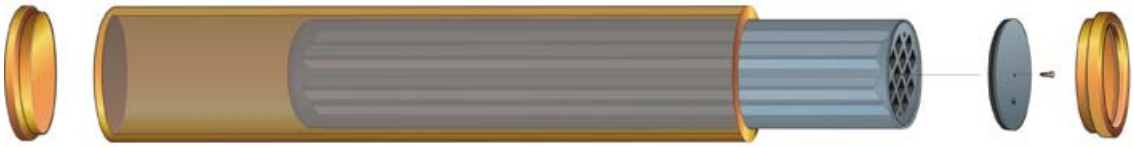

Figure 2-1. *Exploded view of the reference canister and its components (from the left: copper base, copper tube, insert, steel lid for insert and copper lid).*

3 Approach for corrosion assessment

3.1 Strategy

The methodology used in the safety assessment SR-Site is built on experience from earlier safety assessments. The corrosion processes are handled in a way quite similar to the one used in the most recent assessment, SR-Can /SKB 2006/, but with updated supporting documents, improved modelling tools, and site-specific data for hydrology and geochemistry.

An important feature of the safety assessment methodology is the structured and well documented way of handling all processes in the repository system. The methodology must also include strategies for the analysis and modelling efforts, not at least for an efficient use of the resources; the processes that have largest impact on the resulting risk calculations for the repository should be given the largest analysis efforts.

The starting point for the handling of the corrosion processes is the thorough description of all known corrosion processes for copper that could occur in the repository environment. This is documented in the Fuel and canister process report /SKB 2010a/. For all processes there is a description of current knowledge, applied to the specific system and geology, leading to a description of the further treatment in the safety assessment. Already at this stage some processes are excluded from further analysis, for example if the repository environment is not a sufficient prerequisite for the process to occur. A process handled in this way is stress corrosion cracking of copper, where the motive for not treating it further is the required combination of tensile stresses, assisting ions and an oxidative environment. This combination is only conceivable during the early oxic period with elevated temperatures, but it is unlikely that sufficient concentrations of aggressive ions would be available, and there is no evidence that cracking can be sustained during the long-term anaerobic phase in the repository environment /King et al. 2010/.

The next step is to identify processes where the extent of corrosion could be bounded, e.g. by a mass balance approach, where the amount of a specific corrodant is limited, and also in the worst case of letting all the corrodant react with the copper, it will still not cause any major decrease of the copper shell thickness. This mass balance approach is used for e.g. oxygen remaining in the pores of the buffer and backfill (see Section 5.2.2). Other processes could be bounded by the short period they will act on the canister, e.g. corrosion caused by the radiation from the fuel (Section 5.1) or atmospheric oxygen corrosion (Section 5.2.1).

For processes where a mass balance is not limiting, the mass transport of corrodants (or corrosion products) is taken into account. A simple approach would be just to calculate the diffusive transport through the bentonite, but generally the transport resistance for the interface between groundwater in a rock fracture intersecting the deposition hole and the bentonite buffer is more important. For this, the concept of equivalent flowrate, Q_{eq}, is used. This assessment must be done integrated with the evaluation of the geochemical and hydrogeological evolution of the repository. The site specific data for hydrogeology (flow parameters, see Section 4.3.6) and geochemistry (e.g. sulphide concentration in the groundwater, see Section 4.3.5) are used. Further the possibility of erosion of the bentonite buffer (caused by low salinity groundwater) leading to advective conditions around the canister needs to be evaluated in SR-Site.

For the integrated corrosion calculations models using the equivalent flowrate concept have been developed for:

- an intact buffer,
- an intact buffer with a thermally induced spalling zone,
- the combined erosion and subsequent corrosion under advective conditions in the buffer.

The detailed rates of corrosion reactions (reaction kinetics) are pessimistically disregarded in the safety assessment, by assuming that any corrodant reacts immediately as it reaches the canister surface.

For the situation with canisters failing through corrosion, the impact for the repository safety is further assessed by radionuclide transport calculations. For this, the number of failed canisters, together with their specific positions in the repository (to match with the same hydrogeology data as used for the corrosion calculation) will be transferred to the radionuclide transport calculations, to get the risk results that could be compared with the regulatory limits.

3.2 Corrosion reactions

The main corrosion reactions that can take place on the copper in the repository environment is by sulphide

$$2Cu + HS^- + H^+ \rightarrow Cu_2S + H_2 \quad (3\text{-}1)$$

or by oxygen, pessimistically assuming only oxidation to Cu(I)

$$4Cu + O_2 \rightarrow 2Cu_2O \quad (3\text{-}2)$$

This gives the stoichiometric factors for the reactions, i.e. the amount of copper oxidised by one mole of oxidant to

$$f_{HS} = \frac{N_{Cu}}{N_{HS}} = 2 \quad (3\text{-}3)$$

and

$$f_{O2} = \frac{N_{Cu}}{N_{O2}} = 4 \quad (3\text{-}4)$$

3.3 Corrosion depth

The amount of corrodant is converted to copper corrosion depth according to (notation example for sulphide),

$$d_{corr} = \frac{N_{HS} f_{HS} M_{Cu}}{A_{corr} \rho_{Cu}} \quad (3\text{-}5)$$

where N_{HS} is the amount of sulphide, f_{HS} is the stochiometric factor, M_{Cu} is the molar mass of copper, ρ_{Cu} is the density of copper and A_{corr} is area exposed to the corrosion attack. The corrosion from oxygen is calculated correspondingly.

4 Mass transport models

For corrosion to occur corrodants must be available at the metal surface to be corroded, and the mass transport of corrodants could be rate limiting for the corrosion process. Mass transport models could then be used to assess corrosion processes. The same is applicable for non-solid corrosion products, as accumulation could lead to a steady-state where the corrosion stops.

The mass transport models used in SR-Site start from the simple approach just to calculate the diffusive transport through the bentonite, but generally the transport resistance for the interface between groundwater in a rock fracture intersecting the deposition hole and the bentonite buffer is more important, and is limiting. For this, the concept of equivalent flowrate is used /Neretnieks et al. 2010/. The equivalent flowrate can be viewed as the flowrate of groundwater that will be depleted of its solute during the water passage past or through a deposition hole. The inverse of the equivalent flowrate is the transport resistance, i.e. the resistance for a solute to transfer through a system. The models were originally developed to be used in safety assessments for the transport of radionuclides, but are applicable also for transport of other solutes, e.g. corrodants /Neretnieks et al. 2010/.

In the models the concentration of corrodant at the canister surface is pessimistically assumed to be zero. This is a conservative assumption as it gives the largest transport rate. The corrosion reaction is assumed to be infinitely fast, and the overall rate of corrosion is only limited by the rate at which the corrodant can reach the surface of the canister.

In Sections 4.1–4.3 the transport equations are given for the corrosion calculations where mass transfer is limiting the corrosion rate.

4.1 Diffusion – one-dimensional depletion front model

For an intact buffer the molecular diffusion is the dominating mass transport process as the bentonite clay has so low hydraulic conductivity that advection can be neglected /SKB 2010e/.

The rate of diffusion can generally be described by Fick's first law of diffusion

$$J = -D\frac{\partial c}{\partial x} \qquad (4\text{-}1)$$

where J is the flux (expressed in amount per area and time, e.g. mol/m^{2}s), D is diffusivity or diffusion coefficient, c is concentration of solute that diffuses and x is the diffusion distance.

For a steady-state situation with diffusion from a concentration c_0 to a concentration c_1 at the distance x, the mass flux can easily be calculated when the diffusivity D is known.

Simple diffusion calculations are used in SR-Site to evaluate transport of oxygen (remaining in the buffer and backfill) and for diffusion of hydrogen gas (as the result of copper reacting with water) away from the canister. The diffusivity used should be the effective diffusivity in bentonite, $D_{e,buffer,i}$ for the species i.

A simple depletion front model can be used to assess how diffusion would deplete a volume/area/length (depending on geometry) of an initial concentration of a corrodant. This can for example be applied for pyrite in the bentonite dissolving as sulphide, which diffuses to the canister and reacts with the copper.

The bentonite contains a certain concentration of pyrite, FeS_2, corresponding to an equivalent concentration of sulphide, $c_{HS,buff}$ (in kg/m^3), that is sufficient to uphold a constant concentration of sulphide in the bentonite pore water, $c_{HS,pore}$ determined by the chemical environment in the bentonite. Sulphide will however be consumed by corrosion of the copper canister, meaning that the bentonite contents of solid, immobile pyrite will be depleted from the bentonite/canister interface and outward.

Since the initial equivalent concentration $c_{HS,buff}$ is considerably higher than the concentration limit $c_{HS,pore}$ the situation can, in one dimension, be described as a distance x from the canister at time t, within which the buffer is depleted of pyrite. Between the canister surface and x, sulphide will diffuse to the canister, further depleting the buffer of pyrite.

At the front, the flux of sulphide diffusing from the front to the canister is determined by Fick's law

$$\varphi(x) = c_{HS,pore}\frac{D_{e,buffer,HS}A}{x} \tag{4-2}$$

and the front moves with the rate it takes to deplete the concentration of sulphide in the buffer at the specific flux at distance x

$$\frac{dx}{dt} = \frac{\varphi(x)}{c_{HS,buff}A} \tag{4-3}$$

where $D_{e,buffer,HS}$ is the effective diffusion coefficient of sulphide in the buffer, A is the area considered (to get the 1D-flow) and x is the distance of the depleted front to the canister at time t.

Inserting Equation 4-2 in Equation 4-3 and integrating gives the depletion front distance as a function of time

$$x(t) = \sqrt{\frac{2D_{e,buffer,HS}c_{HS,pore}}{c_{HS,buff}}t} \tag{4-4}$$

This model is used for the calculation of depletion of pyrite in the buffer and backfill as well as for a discussion on sulphide from organic materials in the backfill.

4.2 Mass transport for intact buffer with advection in fracture

4.2.1 Conceptual models for the mass transport

The deposition holes for the fuel canisters may be intersected by one or more fractures with seeping water. There are two main processes that govern the rate of solute transport between the seeping water and the canister: in the buffer solutes migrate by molecular diffusion, and in the seeping water transport is also by advection. The hydraulic conductivity in an intact buffer is extremely low /SKB 2010e/, so that molecular diffusion is faster than advective transport within the buffer. The situation will change slightly if there is a zone with higher conductivity, e.g. a thermally induced spalling zone, along the walls of the deposition hole.

Two different models are therefore used, describing the transport of sulphide for a case with fractured rock and a case also including a thermally induced spalling zone. The different pathways for the transport of sulphide are depicted in Figure 4-1. The mass transport of solutes could, with some simplifying assumptions /Neretnieks et al. 2010/ be described with transport resistances, which in turn can be handled in analogy to electrical circuits. The resistances could thus be in series or in parallel. For the derivation of the transport resistances the concept of equivalent flowrate, Q_{eq}, is used. It is a measure of the transport capacity, or expressed in another way, the flowrate of water that could be depleted of (or filled with) a solute of a certain concentration. The equivalent flowrate, Q_{eq}, is the inverse of the transport resistance. Expressions for the equivalent flowrates for the different transport paths are derived in /Neretnieks et al. 2010/ and summarised below.

As given in Figure 4-1 the transport resistance in the case of a fractured rock consists of the transport from the fracture to the buffer ($1/Q_{eqhydro}$) in series with the transport in the buffer, geometrically taking into account that the sulphide is spread out in different directions in the bentonite ($1/Q_{eqgeometric}$). For the case with a thermally induced spalling zone the transport directly from the fracture to the buffer ($Q_{eqhydro}$) is the same as without spalling, but in parallel to transport path through the damaged zone. This combined transport resistance is in series with the diffusion perpendicular through the buffer to the canister surface.

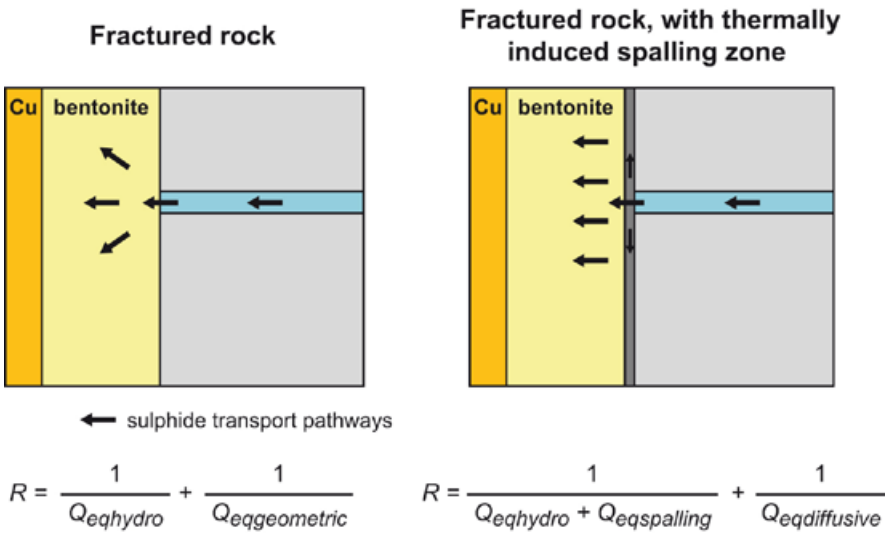

Figure 4-1. *Transport pathways for sulphide for a fractured rock and for fractured rock with a thermally induced spalling zone. The transport resistance could be expressed with the concept of equivalent flowrate Q_{eq}.*

The $\mathbf{1/Q_{eqhydro}}$ term represents transport resistance for the mass transfer from the flowing water in the fracture into the bentonite buffer. The Q_{eq} for this mass transfer is given as /Neretnieks et al. 2010, Equation 3-5/

$$Q_{eqhydro} = 4.51 \cdot \delta\sqrt{D_w r_h v} \qquad (4\text{-}5)$$

where δ is the fracture aperture, D_w is the diffusion coefficient of the solute in water, r_h the radius of the deposition hole and v the water velocity. The factor 4.51 is more exactly derived as $8/\sqrt{\pi}$.

For SR-Site this Q_{eq} is taken from the output from the hydrogeological DFN model for each deposition position, see further Section 4.3.6 and /SKB 2011, Section 10.3.6/. (This transport path is nominated Q1 in the hydrogeological modelling as well as in radionuclide transport calculations).

The $\mathbf{1/Q_{eqgeometric}}$ term represents the transport resistance for the mass transfer in buffer when a very small buffer area is exposed to the solute in the flowing groundwater. The solute that goes from the fracture will encounter an increasingly larger cross section to diffuse through and the resistance decreases the farther from the fracture the solute has diffused. This could also be seen as a spread-out of the solute in the bentonite. It has been shown /Neretnieks et al. 2010, Section 5.2, Neretnieks 1986/ that for typical KBS-3 dimensions this resistance can be described as equal to that in a thin band at the mouth of the fracture. The area of the band is set equal to the fracture opening and the band thickness (extension into the buffer) to a distance about 2–4 times the fracture aperture.

In /SKB 2010b, Appendix G/ it is shown that this resistance can be represented by a plug resistance all around the fracture intersection, so that the area of the plug, A_{plug}, is the fracture opening area

$$A_{plug} = 2\pi r_h \delta \qquad (4\text{-}6)$$

where r_h is the radius of the deposition hole and δ is the fracture aperture.

The length of the plug, l_{plug}, is a factor times the fracture aperture. The $Q_{eqgeometric}$ is thus represented by /SKB 2010b, Appendix G/

$$Q_{eqgeometric} = \frac{D_{e,buffer,i} A_{plug}}{l_{plug}} \qquad (4\text{-}7)$$

where $D_{e,buffer,i}$ is the effective diffusion coefficient in the buffer for species i. The fracture aperture δ is factor both in A_{plug} and l_{plug} and will be cancelled out, and $Q_{eqgeometric}$ is thus independent of the fracture aperture. This is valid for the small apertures found in crystalline rock.

In the SR-Site modelling the ratio A_{plug}/l_{plug} is used directly in the calculation, and set to 5.5/3.1 m. This is derived in /SKB 2010b, Appendix G/ for a fracture aperture δ=10^{-4} m, giving the length of the plug, l_{plug} to $3.1 \cdot 10^{-4}$ m. This plug length corresponds to the band thickness mentioned above, and the factor 3.1 falls in the generally mentioned range of 2–4. The area of the plug for the same fracture aperture will be $5.5 \cdot 10^{-4}$ m^2 ($2\pi \cdot 0.875$ m$\cdot$ $1 \cdot 10^{-4}$ m = $5.5 \cdot 10^{-4}$ m^2).

The $\mathbf{Q_{eqspalling}}$ term (that is added to the Q_{eq} from the hydrogeological modelling) represents the mass transfer between water in a damaged zone of the deposition hole and the buffer. It is expressed as an equivalent flow as /Neretnieks et al. 2010, Equation 4-14/

$$Q_{eqspalling} = q_{zone} \cdot 1.13 \cdot \frac{\sqrt{D_{py} t_{res}}}{d_{zone}} \tag{4-8}$$

where q_{zone} is the flowrate in the spalling zone (calculated from the output of the hydrogeological DFN model), t_{res} is the water residence time and d_{zone} is thickness of the spalling zone. The factor 1.13 is more exactly derived as $2/\sqrt{\pi}$. D_{py} is the pore diffusivity in the y-direction and is derived from D_w and τ_y as /Neretnieks et al. 2010, Equation 4-15/

$$D_{py} = \frac{D_w}{\tau_y^2} \tag{4-9}$$

where D_w is the diffusion coefficient of the solute in water and τ_y is the tortuosity in the y–direction.

According to /Neretnieks et al. 2010, Equations 4-16 and 4-17/ the water residence time t_{res} is given by

$$t_{res} = \frac{L_{zone} W_{zone} d_{zone} \epsilon_{zone}}{q_{zone}} \tag{4-10}$$

where L_{zone}, d_{zone}, ε_{zone} and W_{zone} are the length, thickness, porosity and width of the spalling zone respectively.

Inserting Equations 4-9 and 4-10 in 4-8 gives the equivalent flow rate in the spalling zone

$$Q_{eqspalling} = 1.13 \sqrt{\frac{D_w q_{zone} W_{zone} L_{zone} \epsilon_{zone}}{\tau_y^2 d_{zone}}} \tag{4-11}$$

with the parameters as above.

In SR-Site the flowrate in the spalling zone, q_{zone}, is calculated from the Darcy flux, U_0, given as output of the hydrogeological DFN model. The water flowrate can generally be derived from the product of Darcy flux and a cross section area. The cross sectional area to be used here is the product of the capture width of the zone, $W_{capture}$ and a characteristic height. The capture width of the zone, that is the part of the fracture that gives water to the spalling zone, is pessimistically taken as the length of the intersecting fracture, which in turn is given as the fracture length output from the hydrogeological DFN modelling ($L_{fracture}$, the FLEN parameter in the output, see /Joyce et al. 2010/). The capture width would be at its largest for the extreme case of a vertical fracture and as a maximum about twice the height of the deposition hole /Neretnieks 2006a/. Pessimistically the capture width is thus taken as the smallest value of the fracture length and 16 (twice the deposition hole length set to 8 m). The other cross sectional direction, the height, is set to h_{can} (5 m), as this was the height originally used to calculate the Darcy flux, U_0, from the volumetric flow in hydrogeological DFN modelling. The flowrate in the spalling zone is thus set to

$$q_{zone} = min\left[L_{fracture}, 16\right] U_0 h_{can} \tag{4-12}$$

The $\mathbf{1/Q_{eqdiffusive}}$ term represents the transport resistance for the mass transfer through the buffer, from the spalling zone to the canister surface. The transport geometry can be approximated by considering diffusion in a slab with the thickness of the buffer and the cross sectional area equal to the width of the zone times its length. For the canister geometry Fick's first law gives /Neretnieks et al. 2010, Equation 5-2/.

$$Q_{eqdiffusive} = \frac{D_{e,buffer,i} W_{zone} L_{zone}}{d_{buffer}} \tag{4-13}$$

where $D_{e,buffer,i}$ is the effective diffusion coefficient in buffer for species i, W_{zone} is width of the spalling zone, L_{zone} is the length of the spalling zone and d_{buffer} is the thickness of the buffer.

The **transport resistances** for the different pathways are then combined, in analogy to resistance in electrical circuits, to give the total transport resistance for each case. With Q_{eq} being the inverse of the transport resistance this gives

for fractured rock

$$R = \frac{1}{Q_{eq}} = \frac{1}{Q_{eqhydro}} + \frac{1}{Q_{eqgeometric}} \quad (4\text{-}14)$$

and for rock with a thermally induced spalling zone

$$R = \frac{1}{Q_{eq}} = \frac{1}{Q_{eqhydro} + Q_{eqspalling}} + \frac{1}{Q_{eqdiffusive}} \quad (4\text{-}15)$$

Due to uncertainties in the quantification of the dispersion a more pessimistic approach is suggested in /Neretnieks et al. 2010, Section 4.5/ where all the water in the zone is equilibrated so that $Q_{eq} = q_{zone}$. The total resistance for the case including spalling using this pessimistic assumption is

$$R = \frac{1}{Q_{eq}} = \frac{1}{q_{zone}} + \frac{1}{Q_{eqdiffusive}} \quad (4\text{-}16)$$

4.2.2 Conversion of transport resistance into corrosion rates

From the expression of equivalent flowrate, Q_{eq}, the transported amount of solute can be calculated. The transport models can be applied for corrodants or corrosion products, using the appropriate concentrations, diffusivities and stoichiometric factors. Mostly the models are applied for sulphide as a corrodant, which is described below. The amount of sulphide is thus given by

$$N_{HS} = Q_{eq} \cdot [HS^-] \cdot t \quad (4\text{-}17)$$

where $[HS^-]$ is the concentration of sulphide in the groundwater in the fracture, Q_{eq} is the total equivalent flowrate for the case considered and t is the time considered.

The sulphide is assumed to react with copper at the entire surface, according to Reaction 3-1.

The amount of sulphide is converted to copper corrosion depth according to Equation 3-5 where the corroded area is the cylindrical part of the copper shell such that

$$A = 2\pi r_{can} h_{can} \quad (4\text{-}18)$$

Due to the vertical spread of the solute in the buffer, the corrosion attack will be concentrated to the section of the canister side closest to the fracture. This buffer concentration factor, denominated *BCF*, is derived to be around 7 /Liu 2006, Figure 3/.

The general expression for the highest corrosion rate at the canister side will thus be, inserting the buffer concentration factor and the amount of sulphide as by Equation 4-17:

$$v_{corr} = BCF \cdot Q_{eq} \cdot [HS^-] \frac{f_{HS} M_{Cu}}{2\pi r_{can} h_{can} \rho_{Cu}} \quad (4\text{-}19)$$

However, for the spalling case, the geometry of the interface between the spalled zone and the buffer leads to the following relationship, assuming pessimistically that all mass transfer in the buffer occurs in the slab described in connection with Equation 4-13:

$$v_{corr}^{spalling} = Q_{eq} \cdot [HS^-] \frac{f_{HS} M_{Cu}}{W_{zone} L_{zone} \rho_{Cu}} \quad (4\text{-}19a)$$

4.3 Mass transport for a partially eroded buffer with advection in fracture

4.3.1 Erosion model

For low ionic strength water the bentonite gel expansion into a fracture and the release of colloids is assessed. The loss of buffer material from a deposition hole will lead to cases where advective transport in the buffer need to be considered. The rate of loss can be calculated with the model described by /Neretnieks et al. 2009, Moreno et al. 2010/.

The montmorillonite release rate, $R_{Erosion}$, is found to be proportional to the water velocity v, to the power 0.41 and directly proportional to the aperture δ, according to

$$R_{Erosion} = A_{ero}\delta v^{0.41} \quad (4\text{-}20)$$

where the exponent 0.41 and the constant A_{ero} = 27.2 (yielding the loss rate in kg/yr when the water velocity is given in m/yr and the aperture in m) are fitted data from /Moreno et al. 2010/.

The time to reach advective conditions in the buffer is given by

$$t_{adv} = \frac{m_{buffadv}}{R_{Erosion} f_{tdilute}} \quad (4\text{-}21)$$

where $m_{buffadv}$ is the amount of buffer mass loss required to reach advective conditions, and $f_{tdilute}$ is the fraction of time with groundwater sufficiently dilute for erosion.

4.3.2 Conceptual model for the mass transport for corrosion

For corrosion when advection occurs in the buffer, /Neretnieks et al. 2010, Appendix/ showed that, for a wide range of such conditions the equivalent flowrate, Q_{eq}, used for assessing the migration of corrodants from the groundwater to the canister should be replaced by q_{eb}, the water flux through the part of the fracture that intersects the deposition hole. For high flowrates though, i.e. for $q_{eb} > q_{lim}$ the equivalent flowrate Q_{eq} can be approximated to a square-root expression of q_{eb}, thus giving

for $q_{eb} \leq q_{lim}$

$$Q_{eq} = q_{eb} \quad (4\text{-}22)$$

for $q_{eb} > q_{lim}$

$$Q_{eq} = 1.13 \frac{\sqrt{q_{eb} D_w V_{zone}}}{d_{buffer}} \quad (4\text{-}23)$$

where D_w is the diffusion coefficient of solute in water, V_{zone} is the volume of the eroded buffer, d_{buffer} is the thickness of the buffer and 1.13 is more exactly derived as $2/\sqrt{\pi}$.

In addition, the water flux is increased due to the lost flow resistance in the void from the missing bentonite, and /Neretnieks 2006b/ demonstrated that this effect can be bounded by multiplying the undisturbed flow by a factor f_{conc} = 2. The water flowrate can generally be derived from the product of Darcy flux and cross section area. In the hydrogeological DFN modelling, the Darcy flux, U_0, is calculated from the volumetric flow for a cross section area set to $2r_h h_{can}$ (for a horizontal fracture), why the same area is used here to get the flowrate again. This gives, for the case of an eroded buffer:

$$q_{eb} = f_{conc} U_0 2 r_h h_{can} \quad (4\text{-}24)$$

where f_{conc} is the flow concentration factor, U_0 is the Darcy flux derived from the hydrogeological DFN modelling, r_h is the radius of the deposition hole and h_{can} is the height of the canister.

The derived expression for the flowrate is valid for a horizontal fracture. If the fracture has a longer intersection with the vertical deposition hole than a horizontal fracture, then the flowrate will increase in proportion to the intersection length, but so will the buffer mass loss required for advective conditions and the exposed canister surface. No net effect of taking the fracture angle into account is therefore expected on the erosion and corrosion results.

The corrosion rate is then derived in the same manner as for the intact buffer, by calculating the volume of corroded copper from the amount of sulphide, including a stoichiometric factor for the reaction between copper and sulphide, and dividing by the corroded area and the corrosion time.

$$v_{corr} = Q_{eq} \cdot [HS^-] \frac{f_{HS} M_{Cu}}{\rho_{Cu}} \frac{1}{A_{corr}} \quad (4\text{-}25)$$

where Q_{eq} is the equivalent flowrate, $[HS^-]$ is the concentration of sulphide in the groundwater in the fracture, f_{HS}= 2 is the stoichiometric factor taking into account the reaction of sulphide with copper, M_{Cu} is the molar mass of copper, ρ_{Cu} is the density of copper and A_{corr} the area exposed to corrosion.

4.3.3 Eroded volume and corrosion area

The volume of the eroded buffer, V_{zone}, is approximated to a band with the height h_{zone} around the canister, but only for half of the circumference to account for the erosion and subsequent corrosion taking place mostly on the up-stream side of the deposition hole. The volume of the eroded buffer is thus given by

$$V_{zone} = \frac{h_{zone}\pi\left(r_h^2 - r_{can}^2\right)}{2} \tag{4-26}$$

where h_{zone} is the height of the eroded zone, r_h is the radius of the deposition hole and r_{can} is the radius of the canister. For the buffer lost through the fracture it can be envisaged that the buffer originates from a depleted region that is equally high along the deposition hole wall as deep in the axial direction, i.e. setting h_{zone}=d_{buffer}. This approximation is a bit crude, but imaging the geometry growing with a semicircular cross section would only give a factor π/2 larger volume when the eroded space reaches the canister wall. When growing further, the semicircular shape would soon get lost and the volume would be more rectangular. The estimation of the erosion geometry is not elaborated in detail, but the uncertainties are investigated through the modelling of the corrosion geometry.

The rate of corrosion will depend on the geometry of the eroded buffer section, and in particular on the area of the canister exposed to groundwater, A_{corr}, where a smaller area yields a higher corrosion rate. If buffer erosion occurs, it is likely to continue also after part of the canister surface is first exposed, meaning that the exposed area will grow with time. Again, with the corrosion taking place only on the upstream side of the canister, the exposed area would be

$$A_{corr} = \pi r_{can} h_{corr} \tag{4-27}$$

where r_{can} is the radius of the canister and h_{corr} is the height of the canister exposed to corrosion.

It is firstly assumed that the height of the surface exposed to corrosion is equal to the buffer thickness, d_{buffer} , and that this situation does not change with time. This would correspond to the approximation above for the eroded geometry.

A more detailed depiction of the corroded height to grow with time as the eroded volume grows could be as illustrated in Figure 4-2. Assuming a constant growth rate of a semicircle, the exposed height would grow quickly, and for example have grown to a third of the height corresponding to d_{buffer} already after a few percent longer time than for the erosion to initially touch the canister surface.

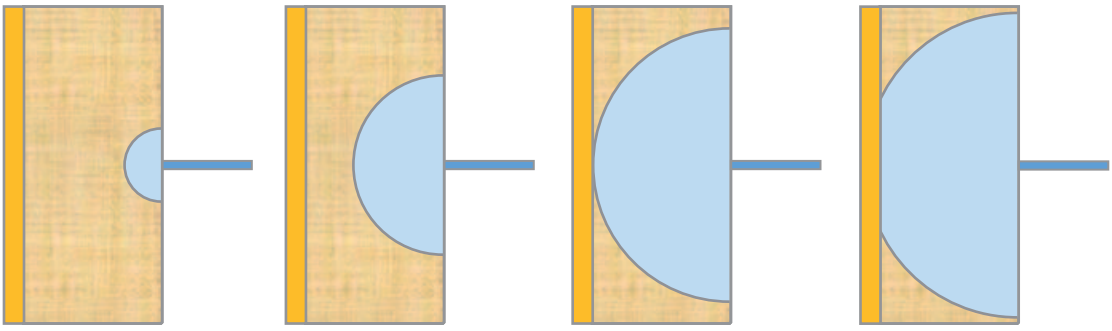

Figure 4-2. *Illustration of the geometry for erosion of buffer, with a growing semi-circular cross section. When the copper surface is reached the eroded section will continue to grow, and expose a larger height of the copper surface.*

As an extreme bounding case the minimum corrosion height is used, taken from the very pessimistic assumption that the erosion stops immediately after it has reached the canister wall. To get the erosion to stop requires the groundwater conditions to abruptly change from dilute to saline. In this case the canister is exposed to corrosion along a line around half its circumference, resembling the first touch of the eroded volume to the canister surface, see Figure 4-3. The corrosion attack is assumed to grow semicircular into the copper, and then the area of this semicircular cross section is set equivalent to a rectangular cross section giving

$$h_{corr} d_{Cu} = \frac{\pi d_{Cu}^2}{2} \tag{4-28}$$

and thus

$$h_{corr} = \frac{\pi d_{Cu}}{2} \tag{4-29}$$

where d_{Cu} is the copper shell thickness. With a copper shell thickness of 5 cm this yields h_{corr}≈0.08 m, to be compared to the use of h_{corr} =d_{buffer}=0.35 m. These approximations of corrosion geometry assume general corrosion. Localised corrosion is a process occurring under oxidation conditions, and then rather in the form of a surface roughness than pits /King et al. 2010/. The case of an eroded buffer occurs when the potential is reducing and further the corrosion by sulphide is in the form of general corrosion, and it is thus not needed to include other geometries than general corrosion.

An upper bound of the corrosion height could be derived from the buffer concentration factor, *BCF*=7, used in the case with an intact buffer discussed in Section 4.2.2. The factor accounts for that the solute transport is concentrated to the section of the canister side closest to the fracture /Liu 2006, Figure 3/. If the mean concentration of solute reaching the canister in its full length instead is concentrated by a factor 7, but keeping the same total amount of solute, this would correspond to it acting on 1/7 of the canister length. Thus the corrosion height would be the canister length 5 m divided by 7, giving h_{corr}≈0.7 m.

In total there is about an order of magnitude between the bounding cases, but the choice of h_{corr}=d_{buffer} is regarded as cautious as the lower value is building on the very extreme case with the erosion stopping when the eroded volume merely has touched the canister. As the erosion volume grows the corrosion height very soon grows larger.

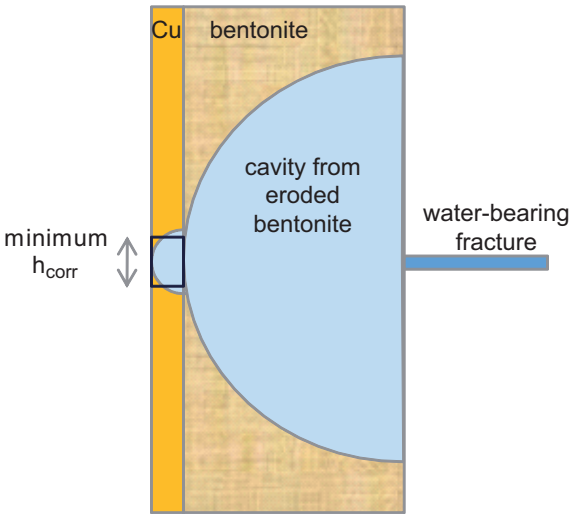

Figure 4-3. *Illustration of the bounding of the corrosion geometry with the minimum corrosion height derived from corrosion of a semicircular hole in the canister wall, for an eroded area just touching the canister surface.*

4.3.4 Copper shell thickness

The extent of corrosion is assessed by comparing the corrosion depth with the initial thickness of the copper shell. The corrosion depth is calculated by

$$d_{corr} = v_{corr} \cdot t \qquad (4\text{-}30)$$

where the corrosion rate is calculated by Equation 4-25 and t is the assessment time. The initial copper thickness, d_{Cu} is taken from the reference design of the canister. The design premise for the copper thickness is specified in /SKB 2009/ and state that there should be "a nominal copper thickness of 5 cm, also considering the welds".

The derivation of the initial state of the copper coverage is based on the reference design, production and control methods described in the canister production report /SKB 2010d/. In short, the minimum copper thickness is 47.5 mm for more than 99 percent of the canisters, while a few canisters per thousand could have a minimum copper coverage of 45–47.5 mm after machining. Small areas with lesser copper thickness (due to defects in the weld or surface defects from transport and handling) can not be excluded, but is not taken into account in the corrosion calculations because of the low probability of the corrosion attack to coincide with these defects. Also, corrosion at surface defects would even out the defects as corrosion proceeds and thus not cause the same reduction of corrosion time as internal defects, which results in a smaller distance to be corroded. The initial copper thickness would also be influenced by initial corrosion by atmospheric oxygen before emplacement and from initially entrapped oxygen, but this is expected to cause corrosion depths less than 500 μm at the most /SKB 2010a/.

A reasonable minimum copper coverage derived from the experiences from the pilot production of the canisters and to be used in the corrosion calculations, is 47 mm, see the SR-Site data report /SKB 2010c/.

More sophisticated analyses are not seen as warranted in light of the considerable uncertainties associated with many other factors in the corrosion calculations, in comparison to the rather limited range of values of initial copper coverage discussed above.

For the assessment of best available technology (BAT) /SKB 2011, Section 14.3.2/ it is though interesting to evaluate the effect of more drastic changes of the copper canister design, and the copper thickness is set to 2.5 and 10 cm respectively.

4.3.5 Sulphide concentration in groundwater

The content of sulphide in groundwaters is controlled by a steady state between microbial sulphate reduction and the processes that remove sulphide: oxidation and precipitation with metals. Under oxidising conditions, for example in superficial waters, sulphide is quickly oxidised to sulphate. Under reducing conditions, dissolved Fe(II) is normally present and the maximum sulphide concentrations are regulated by the precipitation of Fe(II) sulphide according to

$$HS^- + Fe^{2+} = FeS(s) + H^+ \qquad (4\text{-}31)$$

with an equilibrium constant of $K \approx 10^{-3}$. In most groundwaters the Fe(II) concentration is $\geq 10^{-6}$ M, and with a pH between 7 and 8 this gives the maximum sulphide concentration, $[HS^-]$, in the range of 10^{-5} to 10^{-4} M.

Sulphide concentrations in Forsmark were analysed during the site characterisation process and during the subsequent groundwater monitoring. The data are often below the detection limit of the analysis procedure, but in some borehole sections sulphate reduction has taken place during the monitoring period and relatively high sulphide concentrations have been observed. This process has been studied and the conclusion is that accumulated organic gunge and biofilm in the standing monitoring equipment can result in microbial sulphate reduction. It is still not known why this occurs only in some of the monitored sections.

A careful review of all sulphide data has been performed /Tullborg et al. 2010/ and in order to avoid bias due to having many samples in some borehole sections and a few in other locations, a group of samples representing the sulphide concentrations in the different sampling points has been selected,

see Figure 4-4. The maximum sulphide value for Forsmark is $1.2 \cdot 10^{-4}$ M from KFM01D at 343 metres depth. This is, however, an exception and, for practically all of the groundwaters, the sulphide concentration is below $1.3 \cdot 10^{-5}$ M.

No correlation was found between hydrogeological information on the fractures being sampled and the sulphide data. As discussed in /Tullborg et al. 2010/ it may be concluded that sulphide concentrations, including the potential input from methane and hydrogen (as nutrients for sulphate reducing bacteria), and the uncertain contribution from "natural" DOC, will remain at the levels found at present in the Forsmark site. Sulphide concentrations in a given fracture are expected to vary to some extent over a temperate period, but it cannot be concluded that the temporal variations will be sufficiently large that the time averaged concentration would correspond to the average of sulphide concentrations sampled at Forsmark today. The observed distribution of sulphide concentrations in the Forsmark site at present is thus used in the corrosion calculations. Data below the detection limit of the analyses, which is between $9 \cdot 10^{-7}$ and $6 \cdot 10^{-8}$ M, are set to the lowest value in the distribution, $1.2 \cdot 10^{-7}$ M.

In the corrosion calculations for an intact buffer, the 90% percentile of the distribution, $[HS^-] = 1 \cdot 10^{-5}$ M, is used as a constant value over time and for all deposition positions. The extreme choice of using the highest measured value is included as an illustration.

To study the sensitivity of the corrosion results for a partially eroded buffer to the properties of the sulphide distribution some simple changes are done to the distribution, even though there is no reason to pursue the pessimistic approach of using the current measured sulphide any further /SKB 2011, Section 12.6.2, subheading 'Groundwater concentrations of sulphide'/. The analysed cases are:

- The highest point in the distribution i.e. $[HS^-] = 1.2 \cdot 10^{-4}$ M is deleted from the distribution.
- A point with twice the highest, i.e. $[HS^-] = 2.4 \cdot 10^{-4}$ M is added to the distribution.
- The mean value of $[HS^-]$ is used for all deposition positions. This is equivalent to saying that $[HS^-]$ at a given position will vary over time with an average value equal to the mean value of $[HS^-]$ distribution = $5 \cdot 10^{-6}$ M.

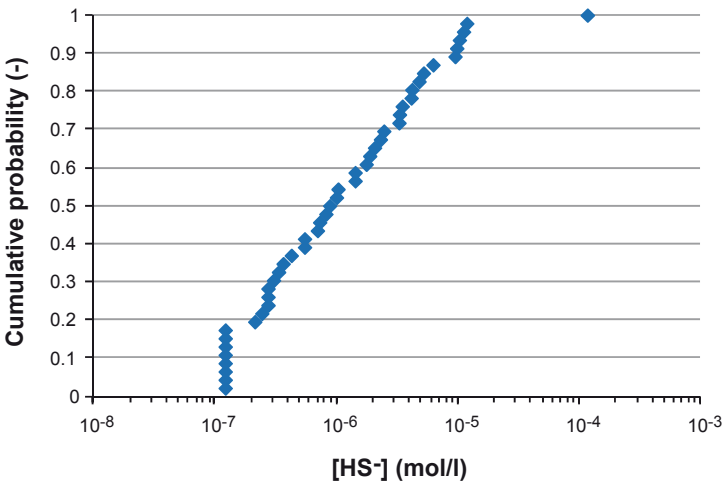

Figure 4-4. *Selected set of sulphide concentrations in contemporary groundwaters of the Forsmark area below 50 m depth /Tullborg et al. 2010/. Data below the detection limit of the analyses, which is between $9 \cdot 10^{-7}$ and $6 \cdot 10^{-8}$ M, are set to the lowest value in the distribution, $1.2 \cdot 10^{-7}$ M.*

4.3.6 Groundwater flow data

The groundwater flow distributions are given by the hydrogeological DFN modelling /SKB 2011, Section 10.3.6/. Three models for the correlation between transmissivity and fracture size are used: fully correlated, uncorrelated and semi-correlated. For each model a first base case realisation is available, with all deformation zones assumed to have only a depth trend of transmissivity, but otherwise constant properties. However, the discrete fracture network is stochastic. In additional realisations, also the deformation zone properties are assumed to be characterised by spatial variability. These realisations are denoted "with stochastic HCD (Hydraulic Conductor Domains)".

A flow distribution consists of the flow situation for each deposition position for a specific realisation with a certain DFN model. For the corrosion assessment flow distributions from all three models variants are used (semi-correlated, correlated and uncorrelated). The base case realisations are used as well as the realisations with stochastic HCD, 10 realisations for the semi-correlated case and 5 each for the uncorrelated and correlated models respectively. For the single parameter sensitivity analysis the model results from the base cases of the DFN modelling are used, while for the sensitivity analyses for the scenario analyses the models including stochastic HCD are used. The hydrogeological data files are listed in the Data report /SKB 2010c, Section 6.7/ and in Appendix 2.

As the time averaged flowrate, q, over the reference glacial cycle is about 80 percent of the values for the temperate period /SKB 2011, Section 10.4.6/, but this is pessimistically disregarded in the erosion/corrosion calculations, where temperate flowrates are used throughout. The "dilute" conditions to give erosion are assumed to occur 25% of the time /SKB 2011, Section 10.4.8/. For the sensitivity analyses also erosion all the time (100%) and initially eroded buffer are analysed.

In the sensitivity analysis for the erosion/corrosion assessment a pessimistic approach for describing fracture aperture is analysed. As described in /SKB 2011, Section 10.3.6/ fracture apertures (δ) are obtained in the hydrogeological model from the fracture transmissivity (T) according to $\delta = 0.5\ T^{0.5}$. An alternative, for buffer erosion more pessimistic relation, discussed in /Joyce et al. 2010, Selroos and Follin 2010/ was also evaluated: $\delta = 0.275 \cdot T^{0.3}$, even though it is dismissed as being unrealistic for the quantification of buffer erosion /SKB 2010c/.

An important parameter for the assessment of erosion and subsequent corrosion is the rejection criteria for deposition positions to be used in the design of the repository as a means to avoid deposition holes with high groundwater flow. Primarily the EFPC (Extended Full Perimeter Intersection Criterion) is used /SKB 2011, Section 5.2.2/, to avoid large fractures to intersect deposition holes. In addition a criterion related to the combination of a high transmissivity and length of the intersecting fracture (T/L filtering) is assumed in the reference design of the repository /SKB 2011, Section 5.2.3/.

5 Corrosion mechanisms

5.1 Gamma radiation

Radioactive decay transforms the radionuclide content of the fuel and radioactive disintegrations generate α-, β-, γ- and neutron radiation as well as new nuclides. The isotopes which dominate during the first few centuries are Cs-137 and Sr-90, both with half-lives of around 30 years. This means the radiation is about 10^{-3} of the initial value after 300 years.

5.1.1 Nitric acid formation

Gamma irradiation of moist air in the canister-buffer gap leads to the formation of nitric acid, which could cause corrosion during the buffer saturation phase. A study by /Jones 1959/ of the nitrogen/oxygen/water homogeneous systems appear to be directly applicable to repository conditions, and found that the formation of nitric acid was linear with the absorbed dose, see further /SKB 2010a, Section 3.5.4, subsection 'Corrosion caused by nitric acid during the buffer saturation phase'/.

If the formation of nitric acid is linear with the absorbed dose, the rate of its formation will be given by:

$$\frac{dN_{HNO_3}}{dt} = \frac{GV_{air}\rho_{air}D_0}{A_v} e^{-ln2\cdot\frac{t}{T_{½}}} \quad (5\text{-}1)$$

and the total amount of produced HNO_3 as a function of time:

$$N_{HNO_3} = \frac{GV_{air}\rho_{air}D_0}{A_v}\frac{T_{½}}{ln2}\left(1 - e^{-ln2\frac{t}{T_{½}}}\right) \quad (5\text{-}2)$$

where G is the G value (in number of molecules/eV), V_{air} the irradiated air volume, ρ_{air} the density of the air, D_o the initial dose rate outside the canister, A_v Avogadro's number, t the irradiation time and $T_{½}$ the half-life (years) of the radiation source.

The irradiated volume is taken as a gap of air, d_{gap}, between the canister and the buffer, giving a volume of

$$V_{air} = h_{Cu}\cdot\pi\left(\left(r_{Cu} + d_{gap}\right)^2 - r_{Cu}^2\right) \quad (5\text{-}3)$$

A gap of 1 cm (d_{gap}=0.01 m) gives the volume 0.161 m^3. With an initial dose rate of 1 Gy/h assumed as ^{137}Cs ($T_{½}$=30), and a G value of 0.02 molecules/eV (from /Jones 1959/), would give a total production of 0.015 moles of nitric acid, which, if consumed uniformly corresponds to a corrosion depth of 7 nm. The calculation is made for the surface that is in direct contact with the water and in maximum radiation field, and should be regarded as a bounding estimate for the corrosion depth.

5.1.2 Radiolysis of water

After water saturation, radiolysis of water near the canister will occur. This will lead to the formation of oxidants and hydrogen. The oxidants can react with copper causing corrosion, see further /SKB 2010a, Section 3.5.4, subsection 'Corrosion by water radiolysis after water saturation'/.

Calculations of radiolysis outside a canister have been made by /Christensen and Pettersson 1997/. An estimate of the maximum possible amount of oxidised copper can be made if one assumes that the oxidation of copper will be as efficient as the oxidation of dissolved Fe(II) in Christensen and Pettersson's calculations. Considering the oxidation of Fe(II) to Fe(III) (as in the calculations of Christensen and Pettersson), after about 317 years (10^{10} s, after which time the gamma dose rate has substantially decreased) the amount of precipitated Fe(III) would be 1 mole per irradiated dm^3 water (value taken from /Christensen and Petterson 1997, Figure 2/). Assuming that the oxidants present in a 5 mm water layer surrounding the canister reach and react with the copper surface, the total volume of irradiated bentonite porewater for a bentonite porosity of 0.4 and canister height h_{can}=4.835 m and radius r_{can}= 0.525 m will be, neglecting the details of the lid and bottom designs:

$$V_{irradiated} = (4.835\cdot 2\cdot 0.525\cdot\pi + 2\cdot 0.525^2\pi)\cdot 0.005\cdot 0.4\ m^3 = 0.035\ m^3 = 35\ dm^3 \quad (5\text{-}4)$$

In Christensen and Pettersson's calculations this would yield a total amount precipitated Fe(III) of 35 moles which would translate into 35 moles of corroded copper. Using Equation 3-5 and the total canister surface area (17.7 m^2) would give a corrosion depth of approximately 14 μm.

5.2 Oxygen

5.2.1 Atmospheric

After the fuel has been encapsulated, the copper canisters will be transported to the geologic repository and deposited, even so some storing time may be inevitable. During that period, the canisters will be exposed to indoor air either at the encapsulation plant or at the repository site and to the atmosphere inside the vessel that will be used for transporting the canister to the repository site.

As described in the updated state-of the-art corrosion report /King et al. 2010/ and summarised in the Fuel and canister process report /SKB 2010a, Section 3.5.4, subsection 'Atmospheric corrosion in the encapsulation plant and repository'/ storing the copper canisters for extended periods of time before disposal for these conditions will have a negligible effect on their service life after disposal. The total corrosion attack even after two years storage will be less than 1 μm. The most likely corrosion product will be copper oxide.

5.2.2 Initially entrapped oxygen

The total extent of corrosion under aerobic conditions will be limited by the available amount of oxygen, i.e. the oxygen trapped in the repository after closure. After backfilling the tunnels, the available trapped oxygen can be calculated from the volumes and porosity of the buffer and backfill. With the tunnel dimensions (w_t=4.2 m, h_t=5.8 m and 6 m spacing between canisters), the porosity of bentonite (ε_{bent}=0.4), the degree of filling (the porosity filled with water to 65% in blocks and 40% in pellets) and the backfill consisting of 60% blocks, 20% pellets and 20% air (assuming the buffer only consisting of blocks) would give a total gas volume of 50.8 m^3 is available per canister:

$$V_{void,backfill} = 4.2 \cdot 5.8 \cdot 6 \cdot \left(0.2 + 0.2 \cdot 0.4 \cdot (1 - 0.4) + 0.6 \cdot 0.4 \cdot (1 - 0.65)\right) = 48.53\ m^3 \quad (5\text{-}5)$$

$$V_{void,buffer} = \left(h_{hole} r_h^2 - h_{can} r_{can}^2\right)\pi \cdot 0.4 \cdot (1 - 0.65) = 2.28\ m^3 \quad (5\text{-}6)$$

With 21% oxygen in air and a gas molar volume of 0.0224 m^3/moles (at 273 K) this gives 455+21=476 moles of oxygen gas.*

Due to the large differences in volume of the buffer in one deposition hole compared to the part of backfill that could be assigned to each deposition hole, only a small part of the oxygen (21 moles) comes from the buffer, and the remainder from the backfill. The entrapped circa 475 moles of oxygen gas corresponds to a corrosion depth of 768 μm if evenly distributed on the canister surface, or 5.5 mm if the oxygen is assumed to attack the lid and topmost 10% of the canister height. It is then pessimistically assumed that copper is only oxidised to Cu_2O.

However, of the available amount of oxygen in the buffer and backfill, only a very small fraction, if any, is expected to reach the canister. The oxygen will most likely be consumed by reactions with accessory minerals. The density of the tunnel backfill is low enough to allow microbial activity and this will also limit the amount of oxygen available for corrosion.

Pessimistic estimates can be done for the possible corrosion depths from entrapped oxygen if these other oxygen consuming processes are disregarded. Evenly distributed corrosion over the canister surface may be a reasonably pessimistic assumption for the oxygen from the buffer, although it is probably more realistic to assume that half of the oxygen will diffuse towards the oxygen free rock. The corrosion from the oxygen in the buffer corresponds to a corrosion depth of 34 μm if all oxygen diffuses inward or 17 μm if half of the oxygen is diffusing outwards.

* The height of the tunnel is 4.8 m and the height of the buffer material in the deposition hole 6.68+1.25=7.93 m /SKB 2010f/. The old values of 5.8 m and 8.5 m respectively, used in these calculations lead to a slightly overestimation of the volume of trapped oxygen in the buffer and backfill.

For the oxygen in the backfill different assumptions could be made that take into account the diffusion of the oxygen. Provided there is a sufficient consumption of oxygen in the rock, the amount of oxygen that could reach the canister will be only the fraction diffusing to the top of the deposition hole. This area ($\pi r_h^2 \approx 2.4$ m^2) is only about 2% of the area of a 6 m tunnel section (the tunnel length assigned to one canister). If it is further assumed that this would only corrode the topmost 10% of the canister (lid and 10% of the canister height) the corrosion depth would be 106 μm. Adding the corrosion from the buffer would give 106+17=123 μm.

Another approach would be to compare the diffusion time for oxygen in the backfill with the total time before anoxic conditions are reached in the repository. With a pessimistic assumption of 300 years /Wersin et al. 1994/ before the oxygen is consumed by mineral reactions and microbial activity, the diffusion length will be in the order of one metre. Assuming the oxygen in a 3 m cylinder of backfill on top of the deposition hole reaching the canister would correspond to a corrosion depth of 260 μm at the topmost 10% of the canister.

During the time period when the oxygen potential is sufficiently high, pitting corrosion is conceivable. Experimental studies of copper corrosion under repository conditions show, however, that the corrosion will have the appearance of uneven general corrosion, and thus that mechanistic models that include the possibilities of pit stifling are more appropriate than statistically based models e.g. using pitting factors. The experimental data indicate that the unevenness around the average corrosion depth may be in the order of ±50 μm, see further the Fuel and canister process report /SKB 2010a, Section 3.5.4, subsection 'Localised corrosion'/.

In conclusion, the corrosion depth from the atmospheric and initially entrapped oxygen is expected to be 500 μm at most.

5.2.3 Oxygen penetration with glacial melt water

Penetration of oxygenated groundwater to the deposition holes is discussed in /SKB 2011, Section 10.4.7/. The issue is ruled out for the reference evolution, but needs to be analysed also for situations with increased flow caused by an ice sheet margin stationary over a repository for longer periods than expected in the reference evolution. In /SKB 2011, Section 12.6.2, subheading 'Oxygen penetration'/ it is described how the degree of oxygen penetration for steady state flow conditions is controlled by: the duration of the steady state episode, the concentration of oxygen at the inlet of the flow paths, the extent to which microbial processes contribute to oxygen consumption, the surface area of the reducing minerals in the rock and the kinetics of their reactions with oxygen, and the transport properties of the recharge flow paths connecting the surface to the deposition holes.

In the evaluation in the corrosion scenario in SR-Site it is pessimistically assumed that the duration of the stationary situation with ice margin above the repository is 1,000 years and that the oxygen concentration of intruding glacial melt water is at the theoretical upper limit of 1.5 mM /SKB 2011, Section 12.6.2, subheading 'Oxygen penetration'/.

For diffusive conditions in the buffer (intact buffer) the model described in Section 4.2.1 is used, with hydrogeology data for the flow conditions calculated for the stationary ice front location yielding the most extensive oxygen penetration, see /SKB 2011, Section 12.6.2, subheading 'Oxygen penetration'/ for further explanations. An oxygen concentration of 1.5 mM is used as well as the stochiometric factor for oxygen, f_{O2}=4 (see Equation 3-4). A 1,000 year exposure to 1.5 mM of O_2 in a fracture intersecting a deposition hole yields a corrosion of about 0.3 mm in the most exposed deposition position in the repository. A thermally induced spalling zone in all deposition holes is also assumed in this calculation. Note that i) all deposition positions are included in this calculation, not only those for which the analysis of oxygen penetration implies that this would be possible and ii) the theoretically maximal oxygen concentration is assumed.

For assumed advective conditions in the deposition hole the corrosion model described in Section 4.2.2 was applied for the deposition positions to which oxygen was calculated to penetrate for the stationary situation mentioned above. The enhanced flowrates calculated for these positions were used in the corrosion calculation. For each of these deposition positions, a specific oxygen concentration was calculated based on the hydrogeological properties of the flow path connecting the surface to the deposition position and assuming an oxygen concentration of 1.5 mM at the surface, see further

/SKB 2011, Section 12.6.2, subheading 'Oxygen penetration'/.The calculations result in a corrosion rate slightly below 6 μm/yr for the deposition position mostly affected by the high O_2 concentration for the stationary ice front location. The following three most affected positions have corrosion rates of 3.6, 1.7 and 0.9 μm/yr respectively. This yields corrosion depths after 1,000 years of at most 6 millimetres.

Furthermore the following are noted:

- The particular position for which the high oxygen concentration occurs is not among those predicted to experience advective conditions in the erosion calculations carried out with the same hydrogeological DFN model (i.e. the base case realisation of the semi-correlated hydrogeological DFN model). This is because the hydrogeological boundary conditions for the two situations are different. Still this pessimistic combination is assumed.
- Only the most unfavourable of the modelled ice front locations results in substantial oxygen penetration. It is assumed here that for the 1,000 year duration of the ice front standstill, the ice margin does not move forth and back distances in the scale of several hundreds of metres. If the ice front should oscillate around its margin position, then the hydrogeological conditions would change in such a way that no single deposition position would be affected by oxygen penetration during any significant period of time.
- Any localised corrosion in connection with oxygen corrosion under glacial conditions would be in the form of uneven general corrosion (rather than true pitting), and as documented in the Fuel and canister process report /SKB 2010a, Section 3.5.4/ the extent of this roughening could be estimated to be some hundred μm, for corrosion depths in the mm scale.

5.3 Sulphide

After all the oxygen has been consumed, sulphide will be the remaining corrodant present in the repository. The sources of sulphide would be dissolution of sulphide minerals in the buffer and backfill, sulphide formed by microbial sulphate reduction in the buffer and backfill and dissolved sulphide in the groundwater (either from dissolution of sulphide minerals in the rock or as a result of microbial reduction of sulphates in the groundwater-rock system). The corrosion of copper by sulphide will proceed with formation of copper sulphide (for simplicity written as Cu_2S even though other non-stoichiometric forms are possible) and molecular hydrogen.

$$2\,Cu + HS^- + H^+ \rightarrow Cu_2S + H_2 \qquad (5\text{-}7)$$

5.3.1 Sulphide from pyrite in buffer and backfill

Corrosion due to sulphide from pyrite initially present in the buffer can be bounded by a simple mass balance estimate. More realistically the estimate of corrosion should include the dissolution of pyrite and the diffusion transport of the sulphide from the pyrite. The time required for complete depletion of this sulphide from the pyrite can be estimated with a simple transport expression involving the diffusivity and the concentration limit of sulphide in the buffer, see Section 4.1.

The initial content of pyrite and the corresponding sulphide content for different buffer materials is given in Table 5-1. The same pyrite and sulphide contents are assumed in calculations for backfill here, as there are no corresponding specifications for backfill materials.

Using a mass balance, and assuming all initially present pyrite in the buffer sections surrounding the canister side attacks the canister side as sulphide, corrosion of 0.1 mm and 0.9 mm copper is obtained for MX-80 and Ibeco-RWC bentonite, respectively. The corresponding values for pyrite in the buffer on top of the canister attacking the canister lid are 0.4 and 2.9 mm, respectively.

For the depletion front model, the diffusivity (effective diffusivity coefficient) and sulphide solubility are used. To analyse the uncertainties in data for these parameters both a reference and a pessimistic set of values are used, see Table 5-2. As reference value the diffusivity of anions is estimated to have an upper limit of $3.0 \cdot 10^{-11}$ m^2/s, while a pessimistic value corresponds to uncharged H_2S, diffusing with the same diffusivity as HTO (tritium labelled water) /Ochs and Talerico 2004/.

Table 5-1. Initial content of pyrite and the corresponding amount of sulphide according to specifications for the different buffer materials /SKB 2010g/.

	MX-80	Ibeco-RWC	Maximum allowed sulphide content in the buffer /SKB 2010g/
Pyrite (FeS_2)	0.07 weight%	0.5 weight%	
Sulphide content	0.0374 weight%	0.267 weight%	0.5 weight%

Table 5-2. Reference values and pessimistic values for diffusivity and sulphide solubility from pyrite in benonite, used in the depletion front model.

	Diffusivity [m^2/s]	Pyrite solubility [mol/dm^3]
Reference value	$3.0 \cdot 10^{-11}$	$1.17 \cdot 10^{-11}$
Pessimistic value	$1.2 \cdot 10^{-10}$	$3.84 \cdot 10^{-9}$

For the solubility of sulphide from pyrite a reference value of $1.17 \cdot 10^{-11}$ mol/dm^3 is used (for an iron concentration of $3.31 \cdot 10^{-5}$ mol/dm^3), with a pessimistic value given by assuming a very low iron content ($1 \cdot 10^{-10}$ moles/dm^3) in the bentonite /Duro et al. 2006/.

If the diffusion is taken into account by using the depletion front model and using reference values for diffusivity and solubility, the result is a corrosion depth of about 1 µm even for the highest allowed pyrite content in the buffer and for an assessment time of 10^6 years, see Table 5-3. These small corrosion depths are nearly independent of geometry, rendering the same corrosion depth at the side and the top. The depletion front penetrates less than 2 cm (even for the lowest pyrite content as in MX-80), thus only pyrite in the very close vicinity of the canister can reach the copper surface.

Using the pessimistic values for diffusivity and solubility the bentonite at the side of the canister would be depleted of pyrite for MX-80. The pyrite on top of the canister would not be depleted in one million years as the depletion front reaches at a maximum 40 cm (for the lowest pyrite content as in MX-80), and thus not allowing time for any pyrite in the backfill to reach the canister. The corrosion depth would be at a maximum 114 µm, even including a factor of 3 for the deposition hole being three times larger than the canister top. In these calculations a dry density of 1,571 kg/m^3 has been used for the bentonite.

Table 5-3. Corrosion depth in an assessment time of 10^6 years caused by pyrite initially present in the buffer using a 1-D diffusion model, for different pyrite contents in the bentonite.

		MX-80	Ibeco-RWC	Maximum allowed sulphide content in the buffer /SKB 2010g/
Reference values for diffusivity and sulphide solubility from pyrite		0.3 µm	0.8 µm	1.0 µm
Pessimistic case with diffusivity as uncharged H_2S and pyrite solubility at low iron content (10^{-10} mol/dm^3).	canister side	9.5 µm depleted in 773 ky	28 µm	38 µm
	straight on canister top	10.4 µm	28 µm	38 µm
	also considering cylinder with width of deposition hole	31 µm	83 µm	114 µm

5.3.2 Sulphide from sulphate reducing bacteria in the buffer and backfill

For the corrosion caused by sulphide produced by sulphate reducing bacteria (SRB) in the bentonite in the buffer and backfill, the assessment is based on the availability of carbon and energy sources in the buffer and backfill, and on experimental data on microbial activity, as described below. The sulphide produced from SRB in the groundwater-rock system is accounted for in the assessment of sulphide in the groundwater (Section 5.3.3)

An inventory of organic materials (including hydrogen gas from corroding iron and steel) and an assessment of their impact on microbial processes has been prepared /Hallbeck 2010/. The amounts of possibly produced sulphide from these sources are small, except for the organics within the bentonite backfill itself, even though there are large uncertainties of the availability of this organics to SRBs /Hallbeck 2010, SKB 2011, Section 10.2.5/.

The organic matter in the backfill bentonite, if all of it were to be used by sulphate reducing bacteria, would correspond to a maximum produced amount of sulphide of about 13,600 moles per canister. To assume such an amount available for corrosion is considered totally unrealistic for several reasons. First, as mentioned above, this type of organic matter would not be easily available for dissolution. Secondly, if it were dissolved, diffusion would limit the transport of either the dissolved organics or any formed sulphide. An illustration of the transport resistance in the bentonite in the backfill could be done by assuming 1D diffusion of sulphide formed at the same location as the organic matter is degraded and dissolved. Using again the simple transport expression for depletion by diffusion results in the depletion front moving 0.5 to 2.8 m in 10^6 years, depending on how the diffusivity (as anions and as uncharged species respectively) and sulphide concentration (10^{-5} and 10^{-4} M respectively) are represented (see also Section 5.3.1). This depletion length should be compared to the length of the adequate tunnel section (3 m, being half the distance between adjacent deposition positions) added to the bentonite on top of the canister (at least 2.5 m). This indicates that only a fraction of sulphide formed in the backfill in the case of microbial activity could reach the canister in the assessment time of 10^6 years. A simple 1D diffusion calculation can be performed to estimate the amount of sulphide that could be transported from a position in the tunnel floor to the canister lid where it causes corrosion. Assuming pessimistically that a sulphide concentration of 10^{-4} M could be maintained in the backfill (disregarding any depletion effects), and with the diffusivity set pessimistically as that for an uncharged species, this would give a corrosion depth of 2 mm if assuming corrosion on the lid and the topmost 10% of the canister height.

All other sources of organic matter in the repository than organics in the backfill bentonite are less and the amounts of sulphide that could possibly be produced are hence insignificant from a corrosion point of view. The organic matter in deposition tunnels and other areas /Hallbeck 2010/ excluding the bentonite organics, corresponds to about 35 moles sulphide per canister. The total organic material in the deposition hole is a factor of 5 lower than the amount in the deposition tunnels, and, again, this is totally dominated by the insoluble organics in the bentonite. Biofilms formed on the rock surfaces, assuming that no cleaning is undertaken before repository closure, would correspond to 11 moles of sulphide per canister from the deposition tunnels. Anaerobic corrosion of rock bolts and other iron components remaining in the repository gives hydrogen gas that could give sulphide via acetogens and sulphate reducing bacteria, as described in /SKB 2011, Section 10.2.5, subsection 'Effects of organic materials and microbial processes'/. The maximum amount of sulphide produced is estimated to be 353 moles sulphide per canister, by a mass balance. The sulphide is assumed to be directly available for corrosion and no account is taken of hydrogen gas diffusion to the groundwater or the reaction of sulphide with the corroded iron, forming iron(II)sulphide. Again, for illustration purposes these maximum values of possibly produced sulphide can be converted to corrosion depths, assuming evenly spread corrosion all around the canister and neglecting all transport processes. In such a comparison 350 moles sulphide per canister corresponds to a corrosion depth of 300 μm, and 35 moles sulphide corresponds to 30 μm.

Another approach for bounding the possible amount of sulphide production is derived from experiments with highly compacted bentonite and natural groundwater at Äspö /Masurat et al. 2010/. The sulphide production, expressed as Cu_xS, was determined for different bentonite densities, see Figure 5-1. The installed buffer density is 1,950–2,050 kg/m^3 /SKB 2011 Section 5.5.3/. At a bentonite density of 2,000 kg/m^3 the highest measured copper sulphide production was $0.034 \cdot 10^{-12}$ moles/mm^2 day, which would correspond to a corrosion depth of 0.18 mm in a 10^6 year period, while at a

bentonite density of 1,800 kg/m^3 the corresponding values are a measured copper sulphide production of $0.42 \cdot 10^{-12}$ moles/mm^2 day, and a corrosion depth of 2.2 mm in a 10^6 year period. However, the experimental conditions were much more favourable for microbial activity than can be expected in the repository as lactate was added to the experiment as a source of energy and organic carbon. The formation of copper sulphide in this type of experiment has also been shown to be dominated by diffusive transport /Pedersen 2010/. In the experiments by /Masurat et al. 2010/ it can thus not be excluded that some of the formed copper sulphide stemmed from sulphide diffusing in from the circulating groundwater, and not only from sulphide produced by microbial activity in the bentonite. The values in Figure 5-1 are thus overestimates of the sulphide production in the bentonite for several reasons. The installed density of the backfill would be only about 1,700 kg/m^3 /SKB 2011, Section 5.6.3/ and microbial sulphate reduction in the bentonite in the backfill could be somewhat higher under these conditions, but would still be very limited, as can be estimated from Figure 5-1.

In total, the pessimistic estimates of corrosion caused by microbial activity in buffer and backfill would sum up to about 3 mm.

The process of sulphide corroding copper is generating hydrogen gas itself according to the reaction

$$2Cu + HS^- + H^+ \rightarrow Cu_2S + H_2 \quad (5\text{-}8)$$

Hydrogen gas is one source of electron donor that could be used by sulphide reducing bacteria, giving sulphide that corrodes copper etc. As the reduction of sulphate requires eight electrons to be transferred to form one sulphide molecule, and one sulphide only give one hydrogen atom, this would give an infinite set of sulphide produced from one hydrogen sulphide molecule

$$N = 1 + \frac{1}{4} + \frac{1}{4} \cdot \frac{1}{4} + \frac{1}{4} \cdot \frac{1}{16} + \ etc \quad (5\text{-}9)$$

This sum has a finite value as, for

$$t_n = ak^{n-1} \qquad (-1 < k < 1) \quad (5\text{-}10)$$

the sum

$$S_n = \frac{a(k^{n-1})}{k-1} \quad (5\text{-}11)$$

is converging to

$$S = \frac{a}{1-k} \quad (5\text{-}12)$$

The amount of copper corroded will thus increase, but at a maximum with a factor

$$\frac{1}{1-\frac{1}{4}} = \frac{4}{3} \quad (5\text{-}13)$$

A requirement for this to happen is though that there are SRBs that are active, either where the hydrogen is formed (at the copper surface) or if the hydrogen is transported away, at some other place. Then the sulphide needs to be transported back to cause corrosion. The assessment of this effect is thus coming back to the limitations of microbial activity and sulphide transport as treated above and in the rest of Section 5.3.3.

The corrosion as a result from sulphide produced by sulphate reducing bacteria in the buffer and backfill can be summarised as

- The amounts of available organic matter (including hydrogen from corrosion of iron and steel) are small and any sulphide produced would have negligible corrosion effects, except for the organic matter in the backfill that can not be neglected from a mass balance point of view.
- Even the installed backfill has a density that highly restricts activity of SRB. Mass transport further limits the possible amount of sulphide produced in the backfill to reach the canister.
- The corrosion depth would be less than 3 mm in 10^6 years, pessimistically assuming the organic material in the backfill is in a form available for the SRBs.

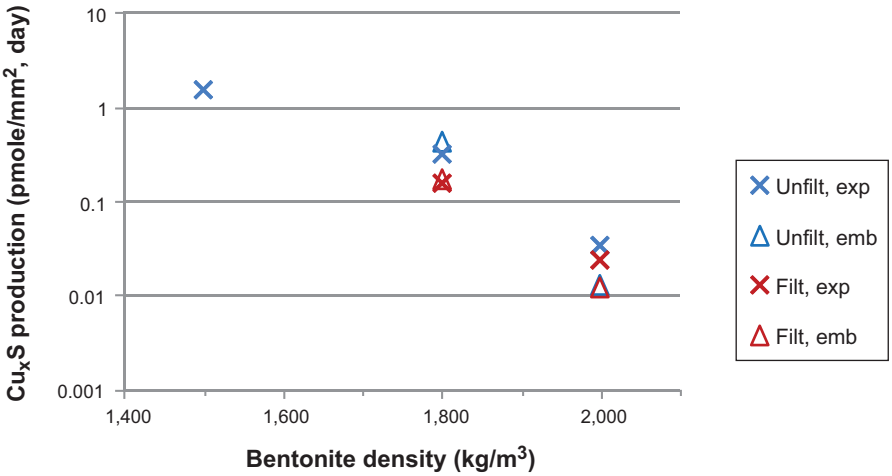

Figure 5-1. *Production rate of Cu_xS on copper test coupons buried in MX-80 bentonite and exposed to unfiltered or sterile-filtered groundwater at the Äspö HRL. The coupons had one end in contact with groundwater (exp) or were fully embedded (emb) (redrawn from /Masurat et al. 2010/).*

5.3.3 Sulphide in groundwater

For sulphide in the groundwater the corrosion is assessed by mass transport limitation. The content of sulphide in groundwaters is controlled by a steady state between microbial sulphate reduction and the processes that remove sulphide: oxidation and precipitation with metals. In Section 4.3.5 it is concluded that the observed distribution of sulphide concentrations in the Forsmark site at present will be used in the corrosion calculations.

The models describing the transport of sulphide from the fracture with flowing, or rather seeping, groundwater to the canister is described in Section 4.2 for an intact buffer and 4.3 for a partially eroded buffer. The results are described in Sections 5.3.4 and 5.3.5 respectively.

5.3.4 Corrosion calculations for intact buffer

Corrosion rate distributions are calculated with the model for intact buffer (see Section 4.2) using a specific sulphide concentration and the flow distributions given by the hydrogeological DFN modelling. A flow distribution consists of the flow situation for each deposition position for a specific realisation with a certain hydrogeological DFN model. The sensitivity of the model for different assumptions on model representation of spalling and on sulphide concentration is performed.

In Figure 5-2 the distribution of corrosion rates for the semi-correlated, uncorrelated and fully correlated hydrogeological base cases are shown, with and without thermally induced spalling. The sulphide concentration is set to $1 \cdot 10^{-5}$ moles/dm^3, which is the 90-percentile of the sulphide distribution measured in Forsmark, see Section 4.3.5. The increase in corrosion rates due to spalling can be seen, as well as the fact that nearly 70% of the deposition positions are not connected to fractures at all (Q1=0). The distributions are corrected for deposition hole rejection criteria (FPC and EFPC, see Section 4.3.6), but in a simplified manner so that these deposition positions are given a no-connective Q1, and thus not are shown in the figure. The number of rejected deposition positions are less than 10% , why the simplification is of no importance for these illustrative calculations.

The pessimistic approach that all the water in the spalling zone could be equilibrated i.e. $Q_{eq}=q_{zone}$ (as described in end of Section 4.2.1) gives the results as shown in Figure 5-3. Comparing Figure 5-2 and 5-3 shows that the more pessimistic approach has minor influence on the maximum corrosion rate, about a factor of two. This more pessimistic approach is therefore not further evaluated.

Even if, totally unrealistically, the highest measured sulphide concentration $1.2 \cdot 10^{-4}$ moles/dm^3 is used the canister would not be penetrated, see Figure 5-4. It must though be pointed out that this data set implies that all deposition holes are exposed to the highest sulphide concentration for the whole assessment time.

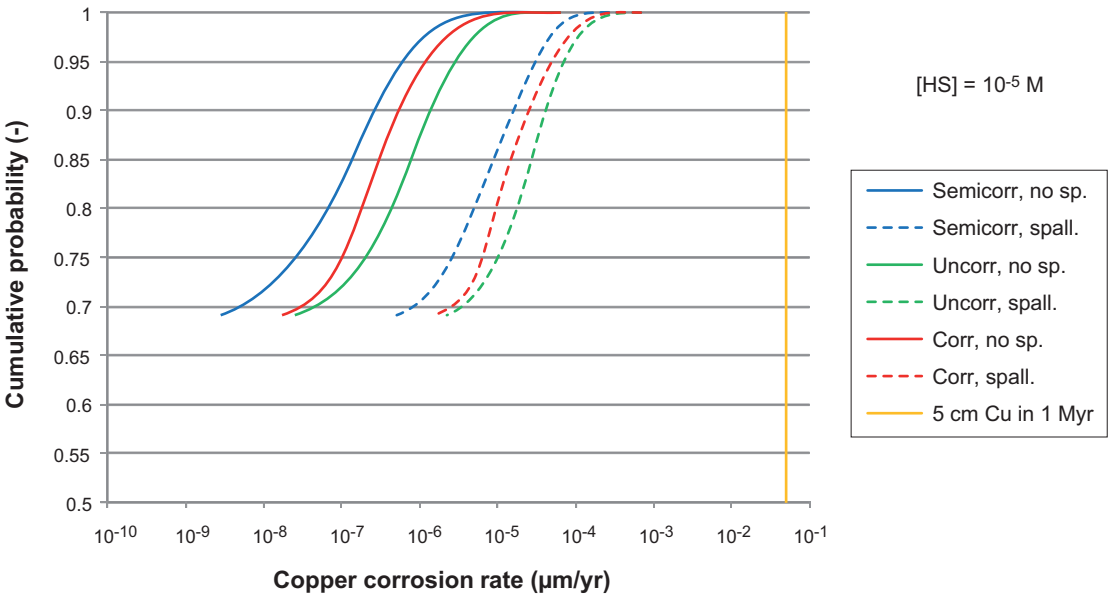

Figure 5-2. *Distribution of corrosion rates for the different hydrogeological DFN models. The effect of a thermally induced spalling zone is shown. The sulphide concentration is set to $1 \cdot 10^{-5}$ moles/dm^3, which is the 90-percentile of the sulphide distribution at Forsmark. Note that nearly 70% of the deposition positions do not have a connected Q1 fracture at all.*

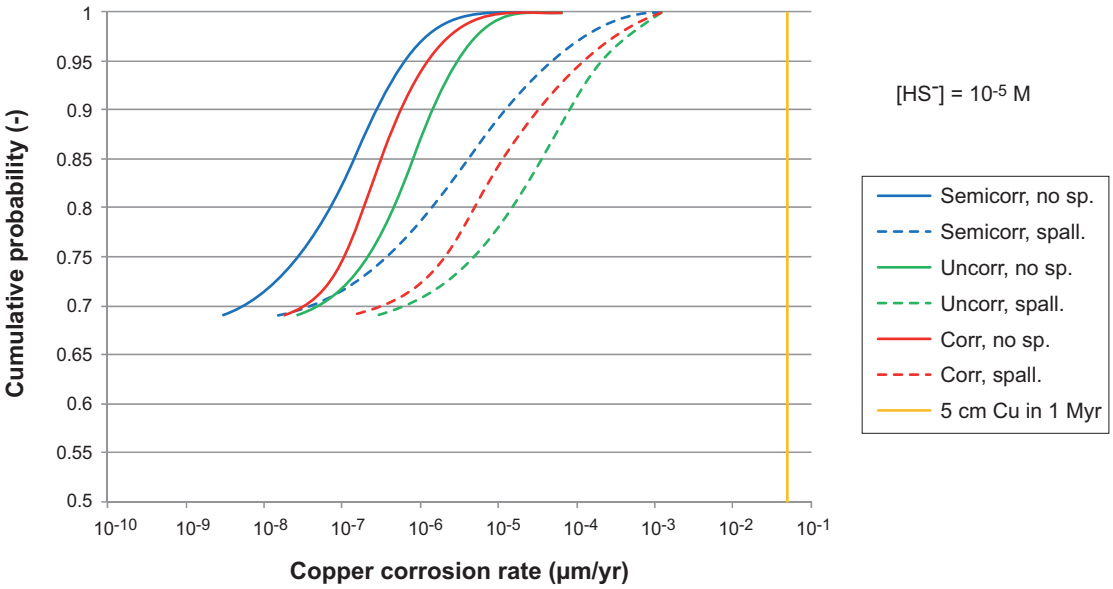

Figure 5-3. *Distribution of corrosion rates for the different hydrogeological DFN models. The effect of a thermally induced spalling zone for the more pessimistic approach that all the water in the spalling zone could be equilibrated is shown. The sulphide concentration is set to $1 \cdot 10^{-5}$ moles/dm^3, which is the 90-percentile of the sulphide distribution at Forsmark. Note that nearly 70% of the deposition positions do not have a connected Q1 fracture at all.*

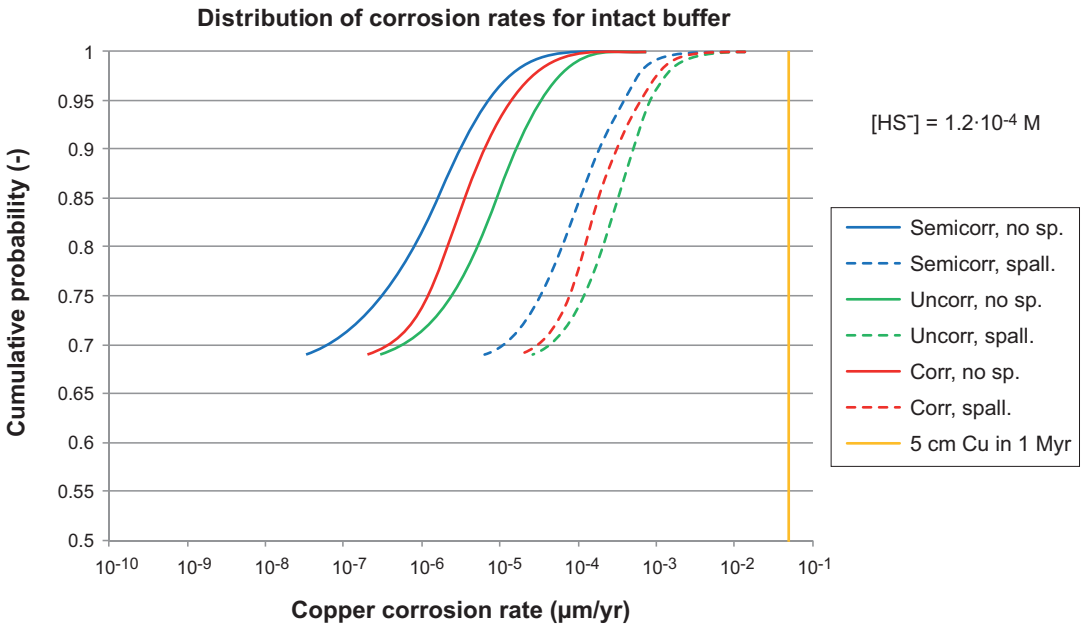

Figure 5-4. *Distribution of corrosion rates for the different hydrogeological DFN models. The effect of a thermally induced spalling zone is shown. The sulphide concentration is set to $1.2 \cdot 10^{-4}$ moles/dm^3, which is the highest sulphide concentration of the sulphide distribution at Forsmark. Note that nearly 70% of the deposition positions do not have a connected Q1 fracture at all.*

The relative influence of the advective and diffusive transport pathways as described in Section 4.2.1 is shown in Figure 5-5. With the same scale as in Figure 5-2 no difference between the curves is visible. By expanding the distribution to show the highest 1% of the corrosion rates the effect of including the diffusive resistance can be seen. For the case with a thermally induced spalling zone the highest corrosion rate is about a factor 2 higher without buffer resistance. If there is no spalling zone, the difference is smaller.

It must also be noted that the corrosion is overestimated in this modelling because:

- If several fractures intersect the deposition hole, the equivalent flowrates for these have been added, which is pessimistic since a partition between several fractures would spread the corrosion attack over the canister area.
- All fractures are assumed to intersect the part of the deposition hole where the canister is located.

The vertical line in Figures 5-2 to 5-5 indicates the corrosion rate that corresponds to a corrosion depth equal to the thickness of the copper canister shell, d_{Cu}=5 cm corroded in 10^6 years. For the sulphide concentration of 10^{-5} M the highest calculated corrosion rate (with a thermally induced spalling zone and taking the buffer resistance into account) is obtained for the fully correlated hydrogeological DFN base case. The corrosion rate corresponds to a corrosion depth of about 0.6 mm in one million years. Without spalling the corresponding corrosion depth is 0.06 mm. It must though be remembered that the sulphide concentration is set constant over time. If the highest measured sulphide concentration was used for all the deposition positions, the corrosion depth would be at the most 7.8 mm for a million year assessment period. This is totally unrealistic and is not used further in the analysis.

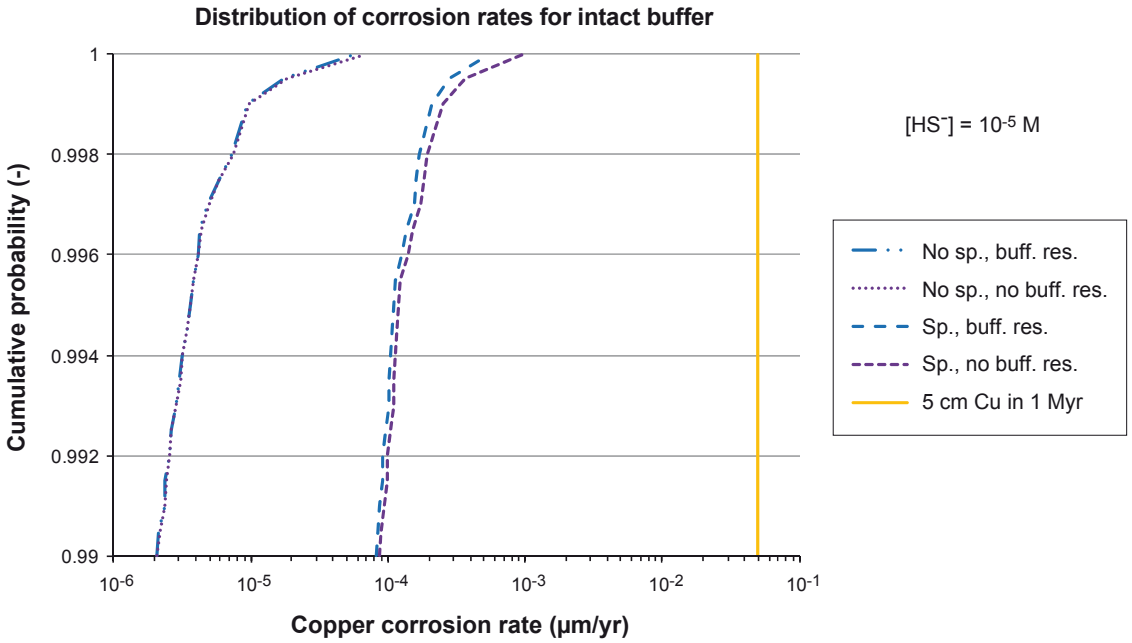

Figure 5-5. *Distribution of corrosion rates for the semi-correlated hydrogeological base case, with and without the transport resistance in the buffer included, for the cases without and with a thermally induced spalling zone. The sulphide concentration is set to 10^{-5} moles/dm^3, which is the 90-percentile of the sulphide distribution at Forsmark.*

5.3.5 Corrosion calculations for a partially eroded buffer

In this section the results from the erosion/corrosion modelling are presented, using the model and data described in Section 4.3.

Model approach

The quantitative evaluations of the hydrogeological evolution /SKB 2011, Section 10.4.6/ indicate that exposure of the buffer to dilute groundwater such that buffer erosion must be considered may occur in the 2 percent of the deposition holes with the highest groundwater flowrates during the 120,000-year glacial cycle and during about 25 percent of the time. As demonstrated in /SKB 2011, Section 10.4.8/ in a small fraction of these deposition holes, buffer may be lost to the extent that advective conditions arise.

First the general type of results is given in Figure 5-6. The sulphide concentration is set constant to $1{\cdot}10^{-5}$ moles/dm^3, which is the 90-percentile of the sulphide distribution measured in Forsmark, see Section 4.3.5. The corrosion rate distribution using the flow distribution from the semi-correlated hydrogeological base case and assuming advective conditions in all deposition positions remaining after rejection according to the EFPC criterion (see Section 4.3.6), is given in Figure 5-6. Also the result when disregarding EFPC rejection is shown in the figure. The copper thickness is set at 47 mm in the modelling of corrosion for advective conditions (see Section 4.3.4) using the more detailed analysis of the initial state than just comparing with the design premise of 5 cm.

For the further calculations, erosion and subsequent corrosion is modelled probabilistically, using distributions of groundwater flow conditions from the hydrogeological DFN modelling and the sulphide distribution for temperate conditions. In the combined erosion/corrosion calculations the time to canister failure is calculated by adding the erosion time to the corrosion time for each position with its specific flow and for a sulphide concentration randomly sampled from the sulphide distribution. In Table 5-4 the erosion and corrosion times are given for the 4 canister positions that could fail within 10^6 years, for the base case semi-correlated hydrogeological DFN model, and by applying the EFPC criterion. In Table 5-5 the corresponding erosion and corrosion times are given for the five canisters that fail within 10^6 years, for realisation r3 of semi-correlated hydrogeological DFN model,

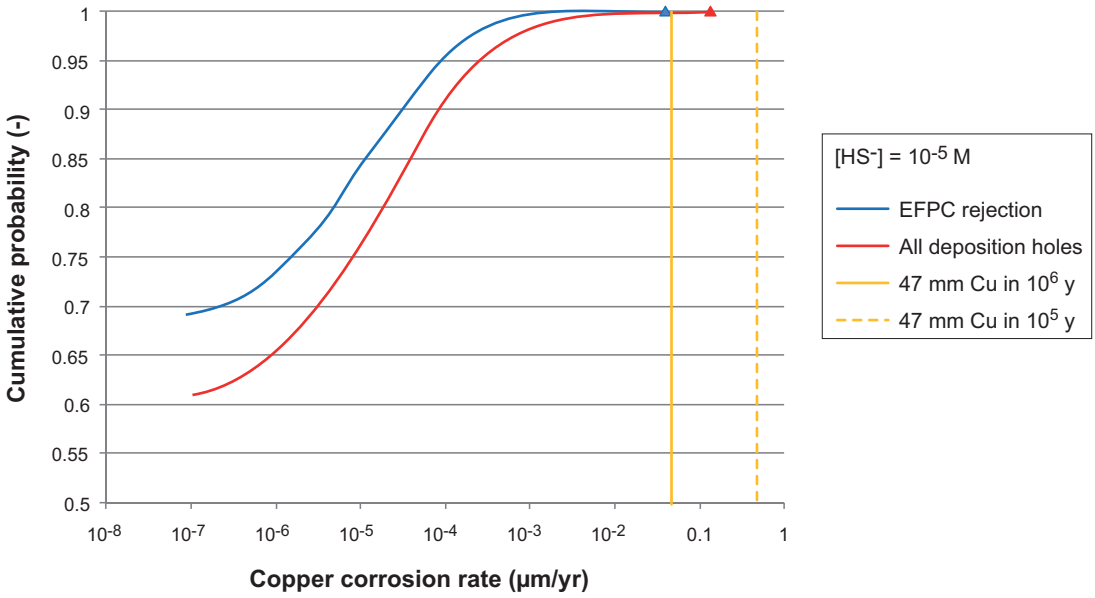

Figure 5-6. Distribution of corrosion rates for the semi-correlated hydrogeological base case assuming advective conditions. The vertical lines indicate the corrosion rates that correspond to corrosion of 47 mm copper in 10^5 (dashed line) and 10^6 (solid line) years respectively.

Table 5-4. Output from the erosion/corrosion model: Deposition hole ID, flowrate, erosion, corrosion and failure time for the 4 canister positions with associated sulphide concentrations, that fail within 10^6 years, for the base case of the semi-correlated hydrogeological DFN model and by applying the EFPC criterion. The possible failures are sorted with the earliest time on top. In this case, failures within 10^6 years only occur for the highest sulphide concentration in the distribution.

Dep. hole ID in DFN hydro model	Flow-rate [m³/yr]	Erosion time [yr]	Sulphide concentration [M]	Corrosion time [yr]	Failure time [yr]
1978	0.144	90,820	0.00012	109,967	200,786
411	0.161	119,733	0.00012	98,482	218,215
6875	0.084	110,655	0.00012	188,485	299,140
401	0.026	278,678	0.00012	607,395	886,073

Table 5-5. Output from the erosion/corrosion model: Deposition hole ID, flowrate, erosion, corrosion and failure time for the 5 canister positions with associated sulphide concentrations, that fail within 10^6 years, for the realisations r3 of the semi-correlated hydrogeological DFN model and by applying the EFPC criterion. The possible failures are sorted with the earliest time on top.

Dep. hole ID in DFN hydro model	Flow-rate [m³/yr]	Erosion time [yr]	Sulphide concentration [M]	Corrosion time [yr]	Failure time [yr]
2026	0.251	104,405	0.00012	75,216	179,621
400	0.079	113,888	0.00012	199,919	313,807
399	0.060	127,696	0.00012	264,285	391,981
398	0.047	141,404	0.00012	338,906	480,309
401	0.042	147,335	0.00012	374,632	521,967
2026	0.251	104,405	1.22E–05	740,617	845,022
2026	0.251	104,405	1.15E–05	786,905	891,310
2026	0.251	104,405	1.06E–05	851,709	956,114

and by applying the EFPC criterion. It can be seen from the tables that the erosion and corrosion times are comparable for the highest sulphide concentration. For lower sulphide concentrations the corrosion times will increase, and thus largely determine the failure times. It is also noted that only a very small part of the distribution of combinations of flowrates and sulphide concentrations will give corrosion rates that can give canister failures in 10^6 years, as also can be seen from Figure 5-6.

The central output from the erosion/corrosion calculations is list of failure times and canister positions resulting from the combination of canister specific flowrates with the sampled sulphide concentrations. These results are transferred to radionuclide transport calculations /SKB 2010b/. Another way of expressing the results from the calculations is the mean number of failed canisters at a certain time (e.g. 10^6 years), which gives an overview of the erosion/corrosion situation.

Sensitivity to hydrogeological DFN model realisations

As a point of departure for the sensitivity analyses, the semi-correlated base case of the hydrogeological DFN model and deposition position rejection according to the EFPC criterion are used. This yields a mean number of failed canisters of 0.087 at one million years when the sulphide distribution is randomly combined with the flowrates for all the deposition positions. Only four deposition holes have sufficiently high flowrates for failure to occur within one million years and for all four, the highest concentration of sulphide in the set of discrete values, $1.2 \cdot 10^{-4}$ M, is required.

From the semi-correlated hydrogeological DFN modelling there are 10 realisations available. As mentioned in Section 4.3.6 the base case differs slightly as it has no stochastic HCD (Hydraulic Conductor Domain). The mean numbers of failed canisters for the different realisations are given separately in Figure 5-7. The rejection criteria give slightly different number of accepted positions in the different realisations, why the output from the erosion/corrosion modelling is normalised to 6,000 canisters, to facilitate the comparison. On average 0.12 canisters fail over a 10^6 years assessment period for the semi-correlated hydrogeological DFN model (average over ten realisations). The same calculation with the five realisations of the uncorrelated and correlated hydrogeological DFN models yield on average 0.65 and 0.57 failed canisters, respectively (see Figure 5-8). The results for the individual realisations can be seen in Figure 5-7. The numbering of the realisations is kept from the hydrogeological model output, where some numbers are omitted.

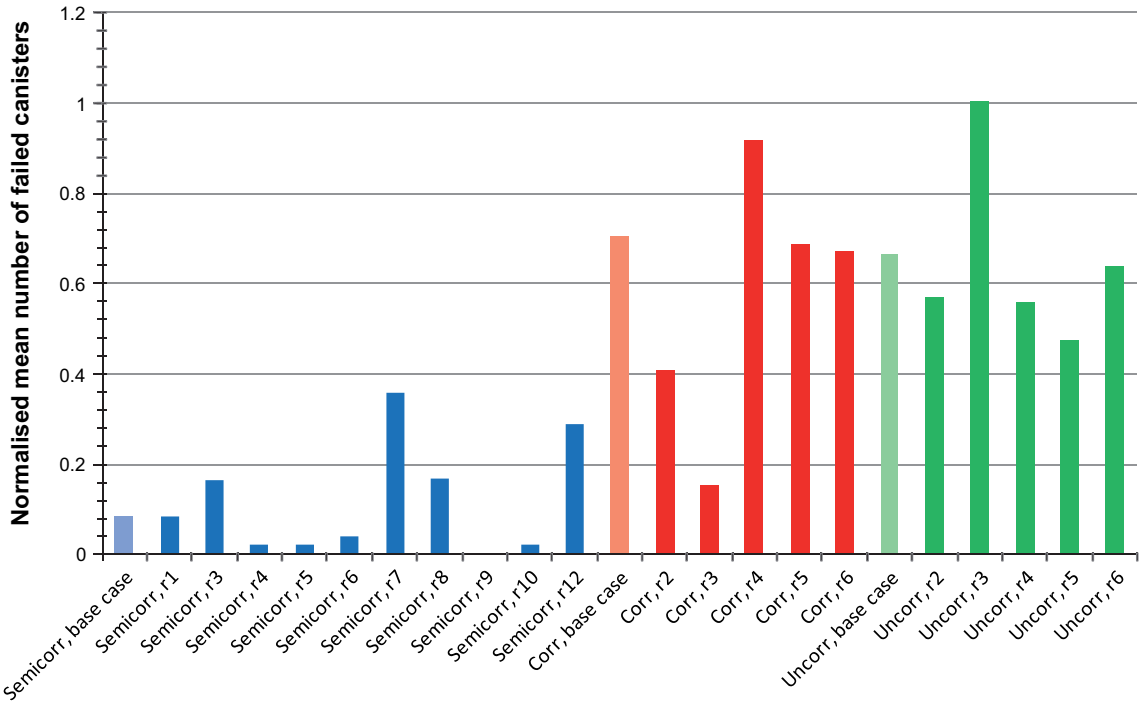

Figure 5-7. *Results from the erosion/corrosion calculations, shown as mean number of failed canisters at 10^6 years, for specific hydrogeological DFN model realisations. Note the linear scale on the y-axis.*

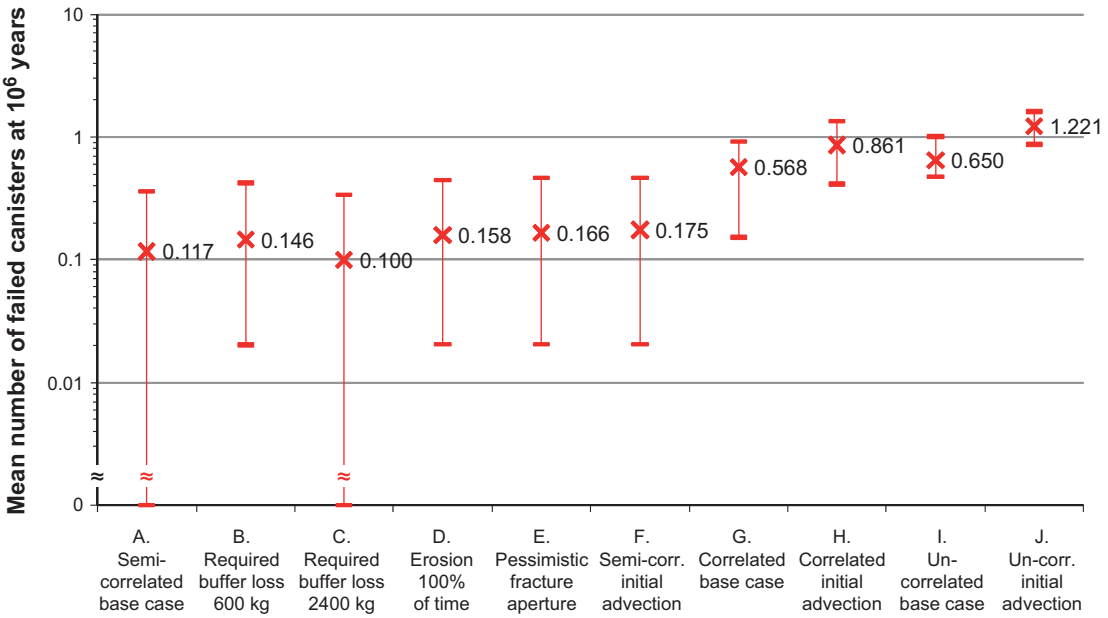

Figure 5-8. *Calculated mean number of failed canisters at 10^6 years for different assumptions in the erosion model. The crosses denote mean values and the bars denote the variability over the several realisations of the hydrogeological DFN models.*

Sensitivity analyses for scenario analysis

The sensitivity calculations for the scenario analysis starts from the semi-correlated hydrogeological DFN model, using the ten realisations with stochastic HCD, with deposition hole rejection according to the EFPC, the site specific sulphide distribution and the cautious corrosion geometry as described in Section 4.3.3. These analyses are used in the evaluation of the corrosion scenario as the central corrosion variant in SR-Site. From the correlated and uncorrelated hydrogeological models the corresponding five realisations (each) are used, also evaluated in the corrosion scenario in SR-Site. The use of these hydrogeological model realisations are denoted "base case" in Figures 5-8 to 5-10, to indicate the starting point for comparisons (and not to allude on the hydrogeological base case realisations).

The sensitivity of the failure times to buffer erosion parameters is shown in Figure 5-8. First the amount of buffer mass loss required to reach advective conditions is varied from 600 kg to 2,400 kg, compared to the base case of 1,200 kg. Further, cases with erosion 100% of the time (instead of 25%), with pessimistic fracture aperture (see Section 4.3.6) as well as initial advection are presented. For the correlated and uncorrelated hydrogeological DFN models the base cases and the cases with initial advection are given respectively.

As seen in Figure 5-8, the sensitivity to all assumptions regarding buffer erosion is limited. The highest impact is obtained for the different hydrogeological DFN models. It is noteworthy that even assuming advective conditions initially in all deposition holes has a limited impact on the extent of corrosion for a given hydrogeological model variant.

Figure 5-9 shows results of the sensitivity to uncertainties in more corrosion related factors, as discussed in Section 4.3.5 (sensitivity related to the distribution of sulphide concentrations) and Section 4.3.3 (corrosion geometry). The cases with changes in sulphide distribution show the following.

- Assuming the mean value of $[HS^-]$ for all deposition positions, which is equivalent to assuming that $[HS^-]$ at a given position will vary over time with an average equal to the mean value of the entire $[HS^-]$-distribution, i.e. $5 \cdot 10^{-6}$ M, yields no corrosion failures for the semi-correlated hydrogeological DFN model. Although it can not be justified to assume a temporal variability that is represented by the given sulphide distribution, it is not unreasonable to assume that the sulphide concentrations would vary over time and thus serve to reduce the expected number of canister failures considerably.

- Omitting or adding another data point with the highest sulphide concentration, i.e. 0.12 mM, has a significant impact on the result. As mentioned above this point is about one order of magnitude higher than the next highest point in the distribution.

These result is a reflection of the fact that canister failures occur only when the highest flowrates are combined with the highest sulphide concentrations, and when both these entities are pessimistically assumed to be constant in time over the entire one million year assessment period for a given deposition position.

Assuming the unrealistic, pessimistic corrosion geometry leads to an increase in the mean number of failed canisters by about a factor of five meaning that the dependence is roughly inversely proportional to the exposed canister surface in this case.

Sensitivity analyses for BAT considerations

For the BAT (best available technique) considerations changes in canister design and repository layout are analysed. The influence of the copper shell thickness is evaluated by changing the reference design copper thickness of 5 cm (47 mm in the base variant calculation) to 10 cm and to 2.5 cm respectively, as part of the BAT considerations. As can be seen in Figure 5-10 an increase of the copper thickness to 10 cm reduces the mean number of failed canisters at 10^6 years by a factor of about 3 while halving the thickness to 2.5 cm increases the number by about a factor of 2.

Also for BAT considerations the importance of the deposition hole acceptance criteria is studied. Two cases are evaluated, with the results shown in Figure 5-10. For the case where the transmissivity-fracture length (T/L) filter is omitted the mean number of failed canisters at 10^6 years is increased by a factor of about 2. If no rejection at all is used, the mean number of failed canisters increases by about a factor of 30.

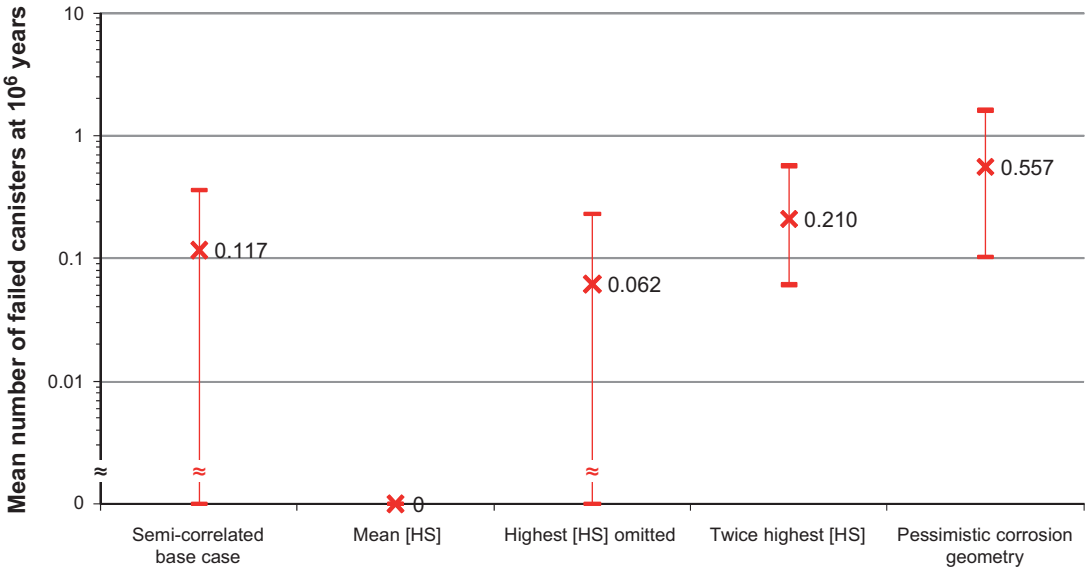

Figure 5-9. *Calculated mean number of failed canisters at 10^6 years to illustrate the sensitivity to other assumptions on sulphide concentration and using a pessimistic corrosion geometry. The crosses denote mean values and the bars denote the variability over the several realisations of the hydrogeological DFN models.*

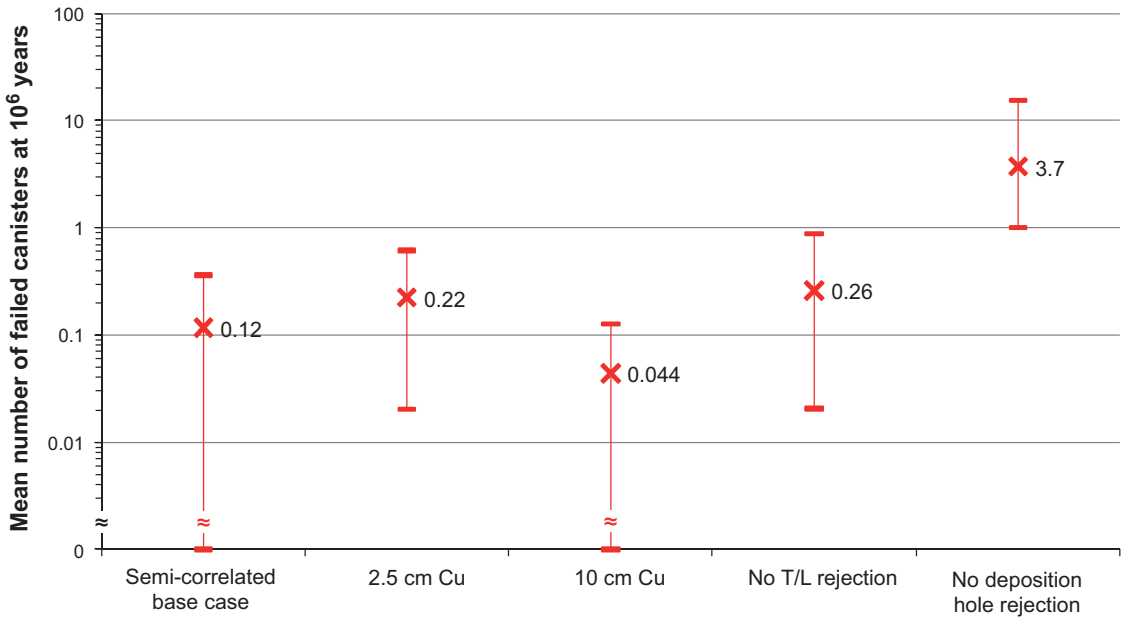

Figure 5-10. *Calculated mean number of failed canisters at 10^6 years to illustrate the sensitivity to changing the copper shell thickness and to applying another deposition hole rejection criterion or using none at all. The crosses denote mean values and the bars denote the variability over the several realisations of the hydrogeological DFN models.*

5.4 What if – corrosion at anoxic conditions with hydrogen gas production

In the Fuel and canister process report /SKB 2010a, Section 3.5.4, subsection 'Corrosion in the absence of oxygen'/ the reaction of copper with water to give a not clearly identified corrosion product and hydrogen gas is discussed. The scientific basis for the suggested reaction is debated, but the consequences for the canister in the repository can be estimated from the published data on hydrogen equilibrium pressure /Szakálos et al. 2007/.

The equilibrium hydrogen pressure is given as $p_{H2}=10^{-3}$ bar.

The gas concentration in water at a certain gas pressure can be derived with Henry's law to

$$c_{H2} = k_H p_{H2} \tag{5-14}$$

where, c_{H2} is the concentration of the gas in water, k_H is a constant specific for the gas and p_{H2} is the partial pressure of hydrogen. For hydrogen gas, k_{H2}=0.78 mol/m^3,bar /Sander 1999/.

After this hydrogen pressure has been reached the corrosion will be limited by transport of hydrogen gas away from the canister. The effective diffusivity of hydrogen in bentonite is very uncertain and thus set to the effective diffusivity of uncharged species (HTO) in bentonite $D_{e,buffer,H2}=1.2\cdot10^{-10}$ m^2/s. With a steady-state zero concentration at the buffer rock interface (diffusion length equal to the buffer thickness) Fick's first law give a transport rate of hydrogen

$$J_{H2} = -D\frac{\Delta c}{\Delta x} = -D_{e,buffer,H2}\frac{k_{H2}p}{d_{buffer}} = 2.67\times10^{-13}\frac{mol}{m^2\cdot s} \tag{5-15}$$

With a stochiometric factor of f_{H2}=2 (2 Cu atoms oxidised for every hydrogen gas molecule formed) the corrosion depth can be estimated by

$$d_{corr} = \frac{N_{H2}f_{H2}M_{Cu}}{A_{corr}\rho_{Cu}} \tag{5-16}$$

Combining Equations 5-15 and 5-16 gives a corrosion depth of 120 µm, for the assessment time of 10^6 years. This estimation is assuming the hydrogen gas is totally consumed outside the buffer (by unspecified processes), and thus that the groundwater contains a zero concentration of hydrogen gas.

Mass transport with flowing (seeping) groundwater can be taken into consideration, and the same models as used for sulphide being transported to the canister can be used for the transport of hydrogen gas from the canister. The parameters to be changed are the diffusivity and the concentration of the species in the groundwater. As a bounding example the model for a partially eroded buffer is used. The flow distribution from the semi-correlated hydrogeological base case is used, and inserting the diffusivity D_{H2}=4.58·10^{-9} m^2/s (instead of 1·10^{-9} m^2/s for sulphide) and the c_{H2}= 7.8·10^{-7} mol/dm^3 (instead of the Forsmark sulphide distribution) in the model results in no failed canisters in 10^6 years. The calculated corrosion depth in the same assessment would be 3.1 mm for the deposition position with the highest flowrate.

For the early phase with an unsaturated buffer the pore space could potentially be filled with hydrogen gas. Using the same assumptions on bentonite porosity and fraction water filled pores in the buffer and backfill, as for the assessment of entrapped oxygen in Section 5.2.2, give the void volume V_{void}=50.8 m^3. The amount of hydrogen gas at a partial pressure of 1 mbar in this volume could be estimated to (assuming an ideal gas at room temperature)

$$N_{H2} = \frac{p_{H2} V_{void}}{R T_{gas}} = \frac{10^{-3} bar \cdot 10^5 \frac{N}{m^2, bar} \cdot 50.8 m^3}{8.314 \frac{J}{mol, K} \cdot 298 K} = 2.05\ mol \qquad (5\text{-}17)$$

This amount of hydrogen corresponds to a corrosion depth of

$$d_{corr} = \frac{N_{H2} f_{H2} M_{Cu}}{A_{corr} \rho_{Cu}} = \frac{2.05\ mol \cdot 2 \cdot 63.55\ \frac{g}{mol}}{17.66\ m^2 \cdot 8.920\ \times 10^6 \frac{g}{m^3}} = 1.7 \times 10^{-6}\ m = 1.7\ \mu m \qquad (5\text{-}18)$$

With pores filled with hydrogen gas the gas will dissolve when in contact with the pore water and further out in the groundwater, and start to diffuse away. For this situation the conditions for the saturated buffer is applicable, and the mass transport models can be used.

Summarising the assessments of the suggested mechanism where copper is corroded by water shows that the corrosion depth is very far from penetrating the copper corrosion shell, even for an assessment time of 10^6 years. It is only in the case of an eroded buffer and then only for the deposition hole with the highest flowrate that the corrosion is in the mm scale.

6 Conclusions on corrosion in SR-Site

For most of the corrosion processes analysed, the corrosion depth is much smaller than the copper shell thickness, even for the assessment time of 10^6 years, as illustrated in Figure 6-1. Several processes give corrosion depths less than 100 µm, but no processes give corrosion depths larger than a few millimetres. The corrosion depths from the different processes could not simply be summed up as their combination requires a far more detailed chemical analysis (as well as statistical analysis regarding the flow and sulphide distributions), but, even if they are cautiously added, the sum is still less than 5 mm.

"What-if"-calculations have been performed to assess the corrosion effect of the suggested reaction of copper with water, in spite of the weak scientific mechanism basis. The results give that the copper shell is very far from being penetrated, even for an assessment time of 10^6 years. It is only in the case of an eroded buffer and then only for the deposition hole with the highest flowrate that the corrosion is in the millimetre scale.

For the case of a partially eroded buffer, the probabilistic calculations show that corrosion could lead to penetration of the copper shell for on average less than one canister, for the assessment time of 10^6 years. Such corrosion extent only comes about for canisters experiencing the most unfavourable combinations of sulphide concentration and flowrates. The calculations give a span of number of failed canisters from zero to less than two penetrated canisters which covers uncertainties regarding the buffer erosion process, the variability in the hydrogeological DFN models and uncertainties in the assumed sulphide concentration distribution, as well as uncertainties in the conceptual model of corrosion geometry (the part of the copper surface that is corroded by the sulphide transported to the canister).

For the eroded buffer case also changes in canister design and repository layout are analysed for BAT (best available technique) considerations. The results show that the number of failed canisters is not very sensitive to a change in canister design (a factor 2 change in copper thickness), while not using the rejection criteria has larger effects.

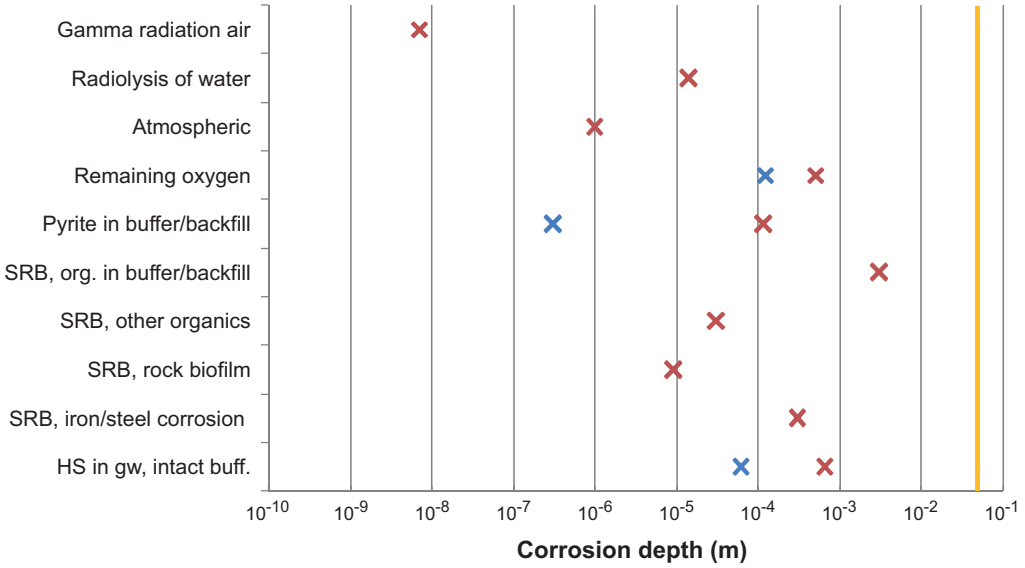

Figure 6-1. *The resulting estimations of corrosion depth from different corrosion processes conceivable in the repository and analysed in the reference evolution in SR-Site, for an assessment time of 10^6 years. None of these processes causes penetration of the copper shell, with marginal. Red crosses represent pessimistic assumptions, while blue crosses represent more realistic assumptions (where calculations are available). The yellow line indicates the copper thickness of 5 cm.*

7 References

SKB's (Svensk Kärnbränslehantering AB) publications can be found at www.skb.se/publications.

Christensen, H, Pettersson, S-O, 1997. Beräkning av radiolys utanför intakt kapsel. Studsvik Report M-97/67, Studsvik Material AB.

Duro, L, Grivé, M, Cera, E, Gaona, X, Domènech, C, Bruno, J, 2006. Determination and assessment of the concentration limits to be used in SR-Can. SKB TR-06-32, Svensk Kärnbränslehantering AB.

Hallbeck L, 2010. Principal organic materials in a repository for spent nuclear fuel. SKB TR-10-19, Svensk Kärnbränslehantering AB.

Jones A R, 1959. Radiation-induced reactions in the N2-O2-H2O system. Radiation Research, 10, pp 655–663.

Joyce S, Simpson T, Hartley L, Applegate D, Hoek J, Jackson P, Swan D, Marsic N, Follin S, 2010. Groundwater flow modelling of periods with temperate climate conditions – Forsmark. SKB R-09-20, Svensk Kärnbränslehantering AB.

King F, Lilja C, Pedersen K, Pikänen P, Vähänen M, 2010. An update of the state-of-the-art report on the corrosion of copper under expected conditions in a deep geologic repository. SKB TR-10-67, Svensk Kärnbränslehantering AB.

Lide D R (ed), 2004. Handbook of chemistry and physics. 85th ed. Boca Raton, FL: CRC Press.

Liu J, 2006. Coupled transport/reaction modelling of copper canister corrosion aided by microbial processes. SKI Report 2006:07, Statens kärnkraftinspection (Swedish Nuclear Power Inspectorate).

Masurat P, Eriksson S, Pedersen K, 2010. Microbial sulphide production in compacted Wyoming bentonite MX-80 under in situ conditions relevant to a repository for high-level radioactive waste. Applied Clay Science, 47, pp 58–64.

Moreno L, Neretnieks I, Liu L, 2010. Modelling of erosion of bentonite gel by gel/sol flow. SKB TR-10-64, Svensk Kärnbränslehantering AB.

Neretnieks I, 1986. Stationary transport of dissolved species in the backfill surrounding a waste canister in fissured rock: some simple analytical solutions. Nuclear Technology, 72, pp 194–200.

Neretnieks I, 2006a. Flow and solute transport in a zone damaged due to spalling. SKB R-06-91, Svensk Kärnbränslehantering AB.

Neretnieks I, 2006b. Flow and transport through a damaged buffer – exploration of the impact of a cemented and an eroded buffer. SKB TR-06-33, Svensk Kärnbränslehantering AB.

Neretnieks I, Liu L, Moreno L, 2009. Mechanisms and models for bentonite erosion. SKB TR-09-35, Svensk Kärnbränslehantering AB.

Neretnieks I, Liu L, Moreno L, 2010. Mass transfer between waste canister and water seeping in rock fractures. Revisiting the Q-equivalent model. SKB TR-10-42, Svensk Kärnbränslehantering AB.

Ochs M, Talerico C, 2004. SR-Can. Data and uncertainty assessment. Migration parameters for the bentonite buffer in the KBS-3 concept. SKB TR-04-18, Svensk Kärnbränslehantering AB.

Pedersen K, 2010. Analysis of copper corrosion in compacted bentonite clay as a function of clay density and growth conditions for sulfate-reducing bacteria. Journal of Applied Microbiology, 108, pp 1094–1104.

Sander R, 1999. Compilation of Henry's law constants for organic and inorganic species of potential importance in environmental chemistry. Mainz: Maz-Planck Institute of chemistry.

Selroos J-O, Follin S, 2010. SR-Site groundwater flow modelling methodology, setup and results. SKB R-09-22, Svensk Kärnbränslehantering AB.

SKB, 2006. Long-term safety for KBS-3 repositories at Forsmark and Laxemar – a first evaluation. Main report of the SR-Can project. SKB TR-06-09, Svensk Kärnbränslehantering AB.

SKB, 2009. Design premises for a KBS-3V repository based on results from the safety assessment SR-Can and some subsequent analyses. SKB TR-09-22, Svensk Kärnbränslehantering AB.

SKB, 2010a. Fuel and canister process report for the safety assessment SR-Site. SKB TR-10-46, Svensk Kärnbränslehantering AB.

SKB, 2010b. Radionuclide transport report for the safety assessment SR-Site. SKB TR-10-50, Svensk Kärnbränslehantering AB.

SKB, 2010c. Data report for the safety assessment SR-Site. SKB TR-10-52, Svensk Kärnbränslehantering AB.

SKB, 2010d. Design, production and initial state of the canister. SKB TR-10-14, Svensk Kärnbränslehantering AB.

SKB, 2010e. Buffer, backfill and closure process report for the safety assessment SR-Site. SKB TR-10-47, Svensk Kärnbränslehantering AB.

SKB, 2010f. Design, construction and initial state of the underground openings. SKB TR-10-18, Svensk Kärnbränslehantering AB.

SKB, 2010g. Design, production and initial state of the buffer. SKB TR-10-15, Svensk Kärnbränslehantering AB.

SKB, 2011. Long term safety for the final repository for spent nuclear fuel at Forsmark. Main report of the SR-Site project. SKB TR-11-01, Svensk Kärnbränslehantering AB.

Szakálos P, Hultquist G, Wikmark G, 2007. Corrosion of copper by water. Electrochemical and Solid-State Letters, 10, pp C63–C67.

Tullborg, E-L, Smellie J, Nilsson A-C, Gimeno M J, Brüchert V, Molinero J, 2010. SR-Site – sulphide content in the groundwater at Forsmark. SKB TR-10-39, Svensk Kärnbränslehantering AB.

Wersin P, Spahiu K, Bruno, J, 1994. Time evolution of dissolved oxygen and redox conditions in a HLW repository. SKB TR 94-02, Svensk Kärnbränslehantering AB.

Appendix 1

Notation and data used

Notation	Description	Data used Value	Unit	Notes	Reference
A_{corr}	Area exposed to corrosion		m^2	Different assumptions	
A_{ero}	Constant in equation for montmorillonite release rate	27.2		Unit, see Section 4.3.1	/Moreno et al. 2010/
A_{plug}	Plug area	$5.5 \cdot 10^{-4}$	m^2		/SKB 2010b, App. G/
A_v	Avogadro's number	$6.022 \cdot 10^{23}$	molecules/ mole		
BFC	Buffer concentration factor	7	–		/Liu 2006/
$c_{HS,buff}$	Total concentration of sulphide in buffer		M	Table 5-1, in weight%	/SKB 2010g/
$c_{HS,pore}$	Concentration of sulphide in pore water		M	Pyrite solubility in Table 5-2	/Duro et al. 2006/
c_{H2}	Concentration of hydrogen gas in water		M	Calculated	
d_{buffer}	Thickness of the buffer	0.35	m		/SKB 2010g, Figure 3-3/
d_{corr}	Corrosion depth		m	Calculated	
d_{Cu}	Copper shell thickness	5 47	cm mm	Intact buffer and eroded buffer respectively	/SKB 2010c, Section 4.1/
d_{gap}	Air gap between canister and buffer	1	cm	Calculated from inner diameter of the ring shaped bentonite blocks and canister diameter	/SKB 2010g, Table 3-4/
d_{zone}	Thickness of the spalling zone	0.1	m		/SKB 2010c, Section 6.5/
D_0	Initial dose rate	1	Gy/h		/SKB 2009/
$D_{e,buffer,i}$	Effective diffusion coefficient in buffer for species i		m^2/s		
$D_{e,buffer,HS}$	Effective diffusion coefficient in buffer for sulphide		m^2/s	Diffusivity in Table 5-2 * Pessimistic value of 10^{-10} used in $Q_{eqdiffusive}$ and $Q_{eqgeometric}$*	/Ochs and Talerico 2004/
$D_{e,buffer,H2}$	Effective diffusion coefficient in buffer for hydrogen gas	$1.2 \cdot 10^{-10}$	m^2/s	Section 5.4	
D_{H2}	Diffusion coefficient of hydrogen gas in water	$4.58 \cdot 10^{-9}$	m^2/s		/Lide 2004/
D_{py}	Pore diffusivity in the y-direction	$1 \cdot 10^{-11}$	m^2/s	Calculated	
D_w	Diffusion coefficient of solute in water	$1 \cdot 10^{-9}$	m^2/s		/SKB 2010c, Section 6.8/
f_{conc}	Flow concentration factor for an eroded buffer	2	–		/Neretnieks 2006/
$f_{tdilute}$	Fraction of time with ground-water sufficiently dilute for erosion	0.25	–		/SKB 2011, Section 10.4.8/
f_{HS}	Stoichiometric factor for reaction with sulphide	2	–	Section 3.2	
f_{H2}	Stoichiometric factor for reaction with water	2	–	Section 5.4	
f_{O2}	Stoichiometric factor for reaction with oxygen	4	–	Section 3.2	
G	G value	0.02	molecules/eV		/Jones 1959/
h_{can}	Height of the canister	4.835	m	Approximated to 5 m in calculations with ero-sion/corrosion model	/SKB 2010d, Table 3-6/
h_{corr}	Height of zone exposed to corrosion		m	Different assumptions	
h_{hole}	Height of deposition hole	8.5	m	Old value, now 7.93 m (see footnote in Section 5.2.2)	

Notation	Description	Data used		Notes	Reference
		Value	Unit		
h_{zone}	Height of eroded zone	$h_{zone}=d_{buffer}$	m	Section 4.3.3	
h_t	Height of tunnel	5.8	m	Old value, now 4.8 m (see footnote in Section 5.2.2)	
J	Diffusive flux			General	
k_{H2}	Constant in Henry's law	0.78	mol/m^3,bar		/Sander 1999/
l_{plug}	Plug length	$3.1\cdot10^{-4}$	m		/SKB 2010d, App. G/
$L_{fracture}$	Length of the fracture		m	Distributions, FLEN i ptb-files	
L_{zone}	Length of the spalling zone	8	m		/SKB 2010c, Section 6.5/
$m_{buffadv}$	Amount of buffer mass loss required to reach advective conditions	1,200	kg	Base case (varied as 600 kg and 2,400 kg in sensitivity anlysis)	
M_{Cu}	Molar mass of copper	63.55	g/mole		
N_i	Amount of specie i		mole	Calculated	
q_{eb}	Flowrate for an eroded buffer		m^3/yr	Calculated	
q_{zone}	Flowrate in the spalling zone		m^3/yr	Calculated	
Q_{eq}	Equivalent flowrate (total)		m^3/yr	General	
$Q_{eqhydro}$	Equivalent flowrate		m^3/y	Distributions, QEQ in ptb-files	
r_{can}	Radius of the canister	0.525	m		/SKB 2010d, Table 3-6/
r_h	Radius of deposition hole	0.875	m		/SKB 2010f, Figure 2-1/
R	Universal gas constant	8.314	J/mole,K		
$R_{Erosion}$	Montmorillonite release rate		kg/yr	Calculated	
s_{can}	Canister spacing	6	m		/SKB 2010f, Section 4.2/
t	Time		yr	General	
t_{adv}	Time to each advective conditions in the buffer		yr	Calculated	
t_{res}	Water residence time		yr	Calculated	
$T_{1/2}$	Half life	30	yr	For ^{137}Cs	/SKB 2010c, Table 3-5/
T	Fracture transmissivity		m^2/s	Calculated	
T_{gas}	Gas temperature		K		
U_0	Darcy velocity		m^3/m^2, yr	Distributions, U0 in ptb-files	
v	Water velocity		m/s	Calculated	
V_{air}	Irradiated volume of air		m^3	Calculated	
V_{void}	Void volume in buffer and backfill		m^3	Calculated	
V_{zone}	Volume of eroded part of buffer		m^3	Calculated	
w_t	Tunnel width	4.2	m		/SKB 2010f, Figure 2-2/
$W_{capture}$	Capture width of the zone		m	Calculated	
W_{zone}	Width of the spalling zone	0.5	m		/SKB 2010c, Section 6.5/
x	Distance from canister to depletion front		m	General equations	
δ	Fracture aperture		m	Different assumptions	
ε_{zone}	Porosity of the spalling zone	0.02	–		/SKB 2010c, Section 6.5/
ε_{bent}	Bentonite porosity	0.4	–	Rounded value	/SKB 2010c, Section 5.1/
φ	Flux (of solute)			Calculated	
ρ_{air}	Density of air	1.184	kg/m^3		
ρ_{Cu}	Density of copper	8,920	kg/m^3		
τ_y	Tortuosity in the y-direction	10	–		/SKB 2010c, Section, 6.5/
$[HS^-]$	Sulphide concentration in groundwater		M	Distribution, or constant value used	/SKB 2010c, Section 6.1/

* The values differ slightly from those recommended in /SKB 2010c, Section 5.3/ and it has been verified that this discrepancy is not influencing the results in any significant way.

Appendix 2

File documentation

The corrosion calculations are archived at SKB as follows:

The erosion/corrosion calculations presented in Section 5.3.5 and 5.4 are using hydrogeological data, i.e. ptb-files, stored in SKBdoc 1256019 ver 1.0 Hydrogeological model data and results – Forsmark. SKB 2010.

The model tool (Excel file) and the result files are stored in SKBdoc 1265612 ver 1.0 Scripts and data used for Analytical erosion corrosion calculations. SKB 2010.

Table A-1 gives an overview of the used hydrogeological and result files.

Mass balance and further mass transport calculations are stored in SKBdoc 1273026 ver 1.0. Further corrosion calculations TR-10-66. SKB 2011.

Table A2-1. Overview of hydrogeologial model files and result files for the erosion/corrosion calculations.

Hydro DFN Model/ realisation	Hydrogeological ptb-file	Converted to Excel file	Result files
Semi-correlated, base case	100615_fs_Q123_2000_pline_merged_ptb.zip	fs_Q1_2000_pline_merged (included in the Excel model file)	BaseRealistions.xlsx
Semi-correlated, r1	100610_fs_r1-10_Q123_2000_pline_merged_ptb.zip	fs_r1_Q1_2000_pline_merged.xlsx	SemiCorrBase.xlsx SemiCorrMBuff600kg.xlsx SemiCorrMBuff2400kg.xlsx SemiCorr100Adv.xlsx SemicorrPessApp.xlsx SemiCorrInitial.xlsx SemicorrMeanHS.xlsx SemicorrOmitHighestHS.xlsx SemiCorrAddTwiceHighestHS.xlsx SemicorrPessCorrgeom.xlsx Semicorr25mmCu.xlsx Semicorr10cm.xlsx SemiCorrNoTFilter.xlsx SemiCorrNoFiltering.xlsx Hydrogenproduction.xlsx
r3	100610_fs_r1-10_Q123_2000_pline_merged_ptb.zip	fs_r3_Q1_2000_pline_merged.xlsx	
r4	100610_fs_r1-10_Q123_2000_pline_merged_ptb.zip	fs_r4_Q1_2000_pline_merged.xlsx	
r5	100610_fs_r1-10_Q123_2000_pline_merged_ptb.zip	fs_r5_Q1_2000_pline_merged.xlsx	
r6	100610_fs_r1-10_Q123_2000_pline_merged_ptb.zip	fs_r6_Q1_2000_pline_merged.xlsx	
r7	100610_fs_r1-10_Q123_2000_pline_merged_ptb.zip	fs_r7_Q1_2000_pline_merged.xlsx	
r8	100610_fs_r1-10_Q123_2000_pline_merged_ptb.zip	fs_r8_Q1_2000_pline_merged.xlsx	
r9	100610_fs_r1-10_Q123_2000_pline_merged_ptb.zip	fs_r9_Q1_2000_pline_merged.xlsx	
r10	100610_fs_r1-10_Q123_2000_pline_merged_ptb.zip	fs_r10_Q1_2000_pline_merged.xlsx	
r12	100610_fs_r1-10_Q123_2000_pline_merged_ptb.zip	fs_r12_Q1_2000_pline_merged.xlsx	
Correlated, base case	100610_fs_corr_Q123_2000_pline_merged_ptb.zip	fs_corr_Q1_2000_pline_merged.xlsx	BaseRealistions.xlsx
Corr, r2	100617_fs_r2_corr_Q123_2000_pline_merged_ptb.zip	100617_fs_r2_corr_Q1_2000_pline_merged.xlsx	CorrBase.xlsx CorrInitial.xlsx
r3	100628_fs_r3_corr_Q123_2000_pline_merged_ptb.zip	100628_fs_r3_corr_Q1_2000_pline_merged.xlsx	
r4	100617_fs_r4_corr_Q123_2000_pline_merged_ptb.zip	100617_fs_r4_corr_Q1_2000_pline_merged.xlsx	
r5	100628_fs_r5_corr_Q123_2000_pline_merged_ptb.zip	100628_fs_r5_corr_Q1_2000_pline_merged.xlsx	
r6	100617_fs_r6_corr_Q123_2000_pline_merged_ptb.zip	100617_fs_r6_corr_Q1_2000_pline_merged.xlsx	
Uncorrelated,base	100610_fs_uncorr_truncHCD_Q123_2000_pline_merged_ptb.zip	fs_uncorr_truncHCD_Q1_2000_pline_merged.xlsx	BaseRealistions.xlsx
Uncorr, r2	100617_fs_r2_uncorr_truncHCD_Q123_2000_pline_merged_ptb.zip	100617_fs_r2_uncorr_truncHCD_Q1_2000_pline_merged.xlsx	UncorrBase.xlsx UncorrInitial.xlsx
r3	100610_fs_r3_uncorr_truncHCD_Q123_2000_pline_merged_ptb.zip	fs_r3_uncorr_truncHCD_Q1_2000_pline_merged.xlsx	
r4	100628_fs_r4_uncorr_truncHCD_Q123_2000_pline_merged_ptb.zip	100628_fs_r4_uncorr_truncHCD_Q1_2000_pline_merged.xlsx	
r5	100628_fs_r5_uncorr_truncHCD_Q123_2000_pline_merged_ptb.zip	100628_fs_r5_uncorr_truncHCD_Q1_2000_pline_merged.xlsx	
r6	100617_fs_r6_uncorr_truncHCD_Q123_2000_pline_merged_ptb.zip	100617_fs_r6_uncorr_truncHCD_Q1_2000_pline_merged.xlsx	